Incorporating Motion of Upper and Lower Platforms: A Generalized Inverse Kinematic Model for Simulation and Experimental Testing of 6-UPS Stewart Platform

M. R. Mohamed
Master of Science in Engineering
Military Technical Collage
Egypt

A. A. Ali
Doctor of Science in Engineering
Military Technical Collage
Egypt

A. A. Roshdy
Doctor of Science in Engineering
Military Technical Collage
Egypt

M. A. Fayed
Professor of Science in Engineering
Military Technical Collage
Egypt

Due to accuracy and precision of parallel manipulators like Stewart platform, several technological applications have relied on them. An accurate kinematic model must be developed in order to improve the manipulator's accuracy. In this paper, inverse kinematic model investigation and verification have been accomplished. Conducting both upper and lower platforms under various motion types is a defining feature of this model. The 3D model of the platform has been directly linked to SimMechanics, paving the way for simulation analysis. MATLAB was used to code the obtained kinematic model. Workspace analysis of the platform has shown the permissible 3D range of each leg, and its intersection consists the total range of the upper platform. Simulation analysis has shown that, position track error hadn't exceeded 10% along any axis, while orientation error hadn't exceeded 2.32% about any axis. In the Experimental model test, the total average error in actuator's displacements is 0.094 cm, while the total average error in rotation angles is 1.145°.

Keywords: *Stewart platform; Parallel manipulator; Inverse Kinematics; Workspace; MATLAB; SimMechanics; Simulation; Experimental model.*

1. INTRODUCTION

Stewart platform is a parallel manipulator with high accuracy, stability and agility. It has attracted attention as it is utilized in various industries, as shown in (Fig. 1), including aerospace and flight simulators, virtual reality and entertainment, precision manufacturing, astronomy and space telescopes, 3D printing and additive manufacturing, robotics and automation, motion simulation and training, medical surgery [1], autonomous vehicle testing and vibration isolation devices. It is also could be used as stabilization platform [2].

Figure 1. Stewart platform applications: (a) flight simulator [3]; (b) AMiBA radio telescope [4]

Kinematic characteristics of a parallel-robot like Stewart platform shown in (Fig. 2) are different from those of serial link mechanisms [5–8]. It has many kinematic constraints issues and a closed loop structure, which is too complicated to be solved by forward (direct) kinematic method [9].

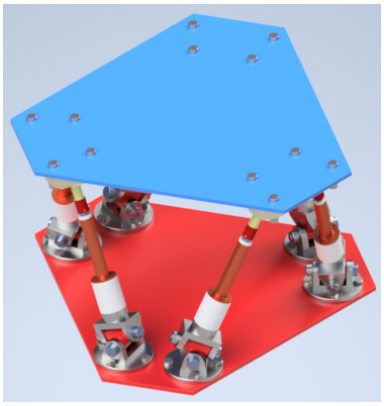

Figure 2. Stewart platform

The kinematic model introduced by Guo, Hongbo and Li, H. in 2006 [10], provided the manipulator velocity and acceleration analysis needed to formulate and derive the dynamic equations. The velocities of centre of gravity of the two (upper and lower) parts of the linear actuator were obtained through the angular velocity of the linear actuator. That angular velocity was derived on the basis that it is perpendicular to leg's longitudinal axis. This approximation was used by many references, but it only simplifies the kinematic equations as it is not always applicable [9].

In the universal-prismatic-spherical (UPS) Stewart platform, angular velocity of linear actuators is resolved

Received: January 2024, Accepted: June 2024
Correspondence to: Mr. Mohamed Raafat Mohamed
Military Technical Collage, Ismail Al-Fangari, El-Qobba Bridge, Cairo, Egypt
E-mail: m.raafat@mtc.edu.eg
doi: 10.5937/fme2403486M

along the universal joint revolution axes into two components [8, 9]. A solution to the kinematic problem introduced by Kalani, Hadi and Akbarzadeh, Alireza in 2016 [11], consists of comparative equations that include each leg unit vector and the rotation matrix of the universal joint of each leg. That solution enabled obtaining the rotation angles of the universal joint. Through deriving the first and second derivatives of these rotation angles, leg's angular velocity and acceleration were obtained respectively.

All the previously mentioned solutions to the Stewart platform kinematic problem consider the upper platform motion while the lower platform remains stationary and rigid with the inertial frame.

Gyroscopic stabilized platforms can only compensate rotational disturbances, and cannot compensate the other transnational disturbances [12,13]. According to D. Stewart article introduced in 1965 [14], both upper and the lower platforms of the Stewart platform are allowed to move in the three-dimensional space freely, and they can make the three types of rotation angles.

Therefore, in sea it is essential to use a complete stabilized platform like Stewart platform, which can compensate motion in all six dimensions for many applications like oceanographic, offshore structures, naval military weapon systems, and ship cranes. That motion-compensation model has an upper stable stationary platform and lower platform is subjected to sea disturbances.

Despite the comprehensive study over the last thirty years in the area of parallel robots like Stewart platform, kinematic analysis presents a deep-rooted complexity. In this study area, additional research must be done. Co-simulation systems research and design and multi-physics simulations should be widely used in this study field to facilitate the study of kinematic problem of parallel robots [15,16].

Mainly, two methods were used to investigate and solve the kinematic problem of Stewart platform. The regular method named forward kinematic method states that the position and orientation of the platform could be obtained according to the leg lengths. The forward kinematic method is too complicated. In addition, given lengths set can result in various configurations. A forward analytical solution is difficult to acquire due to the high coupling and nonlinear properties of the Stewart platform. Many continue to perform extensive studies on the forward kinematics solution. The analytical approach, numerical method, and intelligent algorithm are the most common solutions to the forward kinematics problem. In direct kinematic method a system consists of six sphere coupled nonlinear equations has to be solved because no closed-form of general solution exists [15,17,18]. Maximum number of solutions proved by intersection theory is found to be forty.

Artificial intelligence algorithms were developed around the year 2000 as a result of advances in science and technology, and many researchers employed these algorithms to address the forward problem of the Stewart platform. Neural networks, genetic algorithms, particle swarm optimization algorithms, and other intelligent algorithms are examples. The neural network technique was used by many like Geng and Rahmani to determine the forward kinematics of the Stewart platform. Su, Taherifar and others employed genetic algorithms to optimize the solution, while Zhang and Bingul established a mathematical model of the forward kinematics issue using the particle swarm optimization technique [19].

On the other hand, the second method named inverse (or indirect) kinematic method states that each leg length could be obtained according to a given specific position and orientation of the platform [20, 21]. The main advantage of the inverse kinematic method is being easier than the forward kinematic method.

In order to obtain closed-form solutions, the early development of inverse kinematics for Stewart platforms was mostly dependent on analytical methodologies. These analytical techniques gave precise answers to the inverse kinematics issue, but due to singularities and geometric complexity, they were frequently computationally demanding and difficult to generalize to all configurations [22].

Researchers began investigating numerical ways to effectively tackle the inverse kinematics problem as computer tools and numerical optimization techniques progressed. Iterative algorithms and numerical optimization were two examples of numerical approaches that provided more flexibility and improved handling of singular configurations. Due to their capacity to manage intricate kinematic chains and lessen computing complexity in high-dimensional areas, these approaches have gained popularity.

In both previously mentioned kinematic methods, researchers exerted great effort to conduct accurate equations which were used to define position, velocity, acceleration, rotation angles and singularity analysis of the platform.

This article elaborates on kinematic modeling of the 6-UPS Stewart platform using inverse kinematic method. It covers the mathematical representation and coordinate transformations necessary to describe the motion of the platform considering general motion of both upper and lower platforms. It investigates and verifies an accurate inverse kinematic model for the parallel manipulator, utilizing SimMechanics and MATLAB for simulation analysis and workspace analysis. It validates the derived kinematic model through an experimental model.

The originality of this work is represented by deriving accurate equations for the lengths of the legs, their unit vectors, as well as the required velocity and acceleration for extension and retraction while taking into consideration the motion of both the upper and lower platforms in 3D space. This work also represents the inverse Jacobian matrices associated with the upper and lower platforms. This article also derives the necessary rotation angles for the universal joints to ensure operation within workspace limits. Additionally, it calculates its corresponding angular velocity and angular acceleration.

2. MECHANISM DESCRIPTION

The mechanism under investigation has six extendable legs, an upper platform, and a lower platform. Each leg

is connected to the platform by a spherical joint on the upper platform and a universal joint on the lower platform. The term ”6-UPS” refers to each leg’s upper and lower joints, which are connected by a prismatic joint. The platform is actuated using six linear actuators.

3. INVERSE KINEMATIC MODEL

The UPS Stewart platform is allowed to navigate a space of six degrees of freedom [23] according to the generalized form of the equation developed by Grubler [24] explaining both planar and spatial mechanisms. In this mechanism any intermediate link does not have passive degree of freedom. If any intermediate link has the ability to rotate freely about an axis defined by two joints and cannot transfer torque, then it has a passive degree of freedom. The equation calculates the effective number of degrees of freedom of the mechanism N according to number of degrees of freedom of the space in which the mechanism operates λ, total number of links n, total number of joints j, number of degrees of freedom of each joint F_i^{dof} and number of passive degrees of freedom of the mechanism $I_{passive}$, as follows:

$$N = \lambda(n - j - 1) + \sum F_i^{dof} - I_{passive} \tag{1}$$

The mechanism under investigation has six spherical joints each has 3 degree of freedom, six universal joints each has 2 degree of freedom, six prismatic joints each has 1 degree of freedom, fourteen links (six legs each has fixed and moving parts, a lower platform and an upper platform) and no passive degrees of freedom. Based on the previously mentioned characteristics of links and joints, number of degrees of freedom of the 6-UPS Stewart platform is calculated as follows:

$$N = 6(14 - 18 - 1) + 36 - 0 = 6 \tag{2}$$

The model can do both translation and rotation in 3D space. The key point in investigating and deriving the inverse kinematics of the Stewart platform is studying the kinematic analysis of one leg. Putting into consi–deration that, the upper and lower platforms are initially horizontally orientated and parallel to each other, as shown in (Fig. 3).

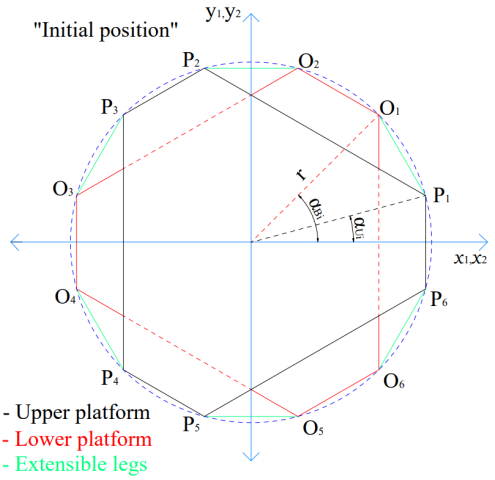

Figure 3. Top view of Stewart platform model initial position

As shown in (Fig. 4) initially the lower platform frame {B} with centre O_B and axes [x_1–y_1–z_1] is para–llel to the upper platform frame {U} with centre O_U and axes [x_2–y_2–z_2] and both are initially parallel to the ab–solute frame {abs} with centre O_{abs} and axes [x–y–z]. Mass centres of the upper and lower platforms coincide on centres of the upper and lower platforms frames respectively. The leg frame {f_i} with axes [x_{3i}–y_{3i}–z_{3i}] is attached to the ith leg at the connection point with the lower platform O_i. z_{3i} axis is always directed along leg position vector directed from O_i to the leg connection point with the upper platform P_i. Other two axes x_{3i} and y_{3i} are directed along the rotational axis of the universal joint.

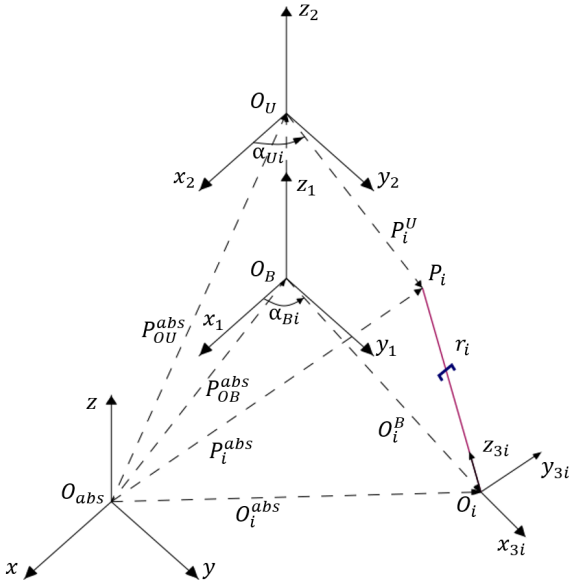

Figure 4. Model coordinates and frames in initial position

2.1 Leg length

Stewart platform is a parallel robot which can track a definite path efficiently with high precision. Leg length calculation and analysis are very important steps in deriving the kinematic model of the platform.

As shown in figure (Fig. 3) the position vector of each leg $\vec{r}_i$, could be derived considering that position of the leg tip with respect to the absolute frame is $\vec{O}_i^B = r\cos(\alpha_{Bi})\hat{i}_1 + r\sin(\alpha_{Bi})\hat{j}_1$, position of the leg $\vec{P}_i^U = r\cos(\alpha_{Ui})\hat{i}_2 + r\sin(\alpha_{Ui})\hat{j}_2$ bottom with respect to the absolute frame is $\vec{O}_i^{abs}$, rotation matrix of upper platform is R_U^{abs}, rotation matrix of lower platform is R_B^{abs}, position vector of the ith leg tip connection with the upper platform with respect to its local frame is $\vec{P}_i^U$, position vector of the ith leg bottom connection with the lower platform with respect to its local frame is $\vec{O}_i^B$, position vector of ith leg tip with respect to upper platform centre in the absolute frame is $\vec{q}_i^{abs}$, position vector of ith leg bottom with respect to lower platform centre in the absolute

frame is $\vec{S}_i^{abs}$, position of upper and lower centre of the platforms with respect to the absolute frame are $\vec{P}_{OU}^{abs}$ and $\vec{O}_{OB}^{abs}$ respectively, as shown in equations 3,4 and 5.

$$\vec{r}_i = \vec{P}_i^{abs} - \vec{O}_i^{abs} \tag{3}$$

$$\begin{aligned} \vec{P}_i^{abs} &= R_U^{abs}\vec{P}_i^U + \vec{P}_{OU}^{abs} \\ \vec{q}_i^{abs} &= R_U^{abs}\vec{P}_i^U \end{aligned} \tag{4}$$

$$\begin{aligned} \vec{P}_i^{abs} &= \vec{q}_i^{abs} + \vec{P}_{OB}^{abs} \\ \vec{O}_i^{abs} &= R_B^{abs}\vec{O}_i^B + \vec{O}_{OB}^{abs} \\ \vec{S}_i^{abs} &= R_B^{abs}\vec{O}_i^B \end{aligned} \tag{5}$$

$$\vec{O}_i^{abs} = \vec{S}_i^{abs} + \vec{P}_{OB}^{abs}$$

Connection points of legs with upper and lower platforms are located on a circular circumference with radius r and make constant angles α_{Ui} and α_{Bi} with x_2 and x_1 axes, respectively, and rotate about z_2 and z_1 axes in [x_2, y_2] and [x_1, y_1] planes, respectively. The position vector of the ith leg connection with the upper and lower platforms with respect to its local frames could be derived as follows:

$$\begin{aligned} \vec{O}_i^B &= r\cos(\alpha_{Bi})\hat{i}_1 + r\sin(\alpha_{Bi})\hat{j}_1 \\ \vec{P}_i^U &= r\cos(\alpha_{Ui})\hat{i}_2 + r\sin(\alpha_{Ui})\hat{j}_2 \end{aligned} \tag{6}$$

Position vector of the upper platform $\vec{P}_{OU}^{abs}$, local rotations of upper platform frame θ_{OU} and total position and orientation vector of the upper platform q_U could be derived as follows:

$$\vec{P}_i^{abs} = \begin{bmatrix} P_{ix}^{abs} \\ P_{iy}^{abs} \\ P_{iz}^{abs} \end{bmatrix} = \begin{bmatrix} q_{ix}^{abs} + x_{OU} \\ q_{iy}^{abs} + y_{OU} \\ q_{iz}^{abs} + z_{OU} \end{bmatrix} = T_U^{abs} \begin{bmatrix} P_{ix}^U \\ P_{iy}^U \\ P_{iz}^U \end{bmatrix} \tag{7}$$

$$T_u^{abs} = \begin{bmatrix} R_U^{abs} & P_{OU}^{abs} \\ 0_{1\times 3} & 1 \end{bmatrix}$$

Position vector of the lower platform $\vec{P}_{OB}^{abs}$, local rotations of lower platform frame θ_{OB} and total position and orientation vector of the lower platform q_B could be derived as follows:

$$\begin{aligned} \vec{P}_{OB}^{abs} &= \begin{bmatrix} x_{OB} & y_{OB} & z_{OB} \end{bmatrix}^T \\ \theta_{OB} &= \begin{bmatrix} \theta_{OBx} & \theta_{OBy} & \theta_{OBz} \end{bmatrix}^T \\ q_B &= \begin{bmatrix} x_{OB} & y_{OB} & z_{OB} & \theta_{OBx} & \theta_{OBy} & \theta_{OBz} \end{bmatrix}^T \end{aligned} \tag{8}$$

The eight frames {B}, {U} and {f_i} have three different basic orientations z_1–y_1–x_1, x_2–y_2–z_2 and z_{3i}–x_{3i}–y_{3i} respectively. The rotation matrices R_B^{abs}, R_U^{abs} and $R_{f_i}^{abs}$ are used to transfer position vectors from the body frame to the absolute frame xyz. The three formulas of rotations matrices are derived as follows:

$$\begin{aligned} R_B^{abs} &= R_z(\theta_{OBz})R_y(\theta_{OBy})R_x(\theta_{OBx}) \\ R_U^{abs} &= R_x(\theta_{OUz})R_y(\theta_{OUy})R_z(\theta_{OUx}) \\ R_{f_i}^{abs} &= R_z(\alpha_{Bi})R_x(\psi_i)R_y(\gamma_i) \end{aligned} \tag{9}$$

The final form of position vector for the upper connection point, could be derived considering that the transformation matrix of the upper platform is T_U^{abs}, as follows:

$$\vec{P}_i^{abs} = \begin{bmatrix} P_{ix}^{abs} \\ P_{iy}^{abs} \\ P_{iz}^{abs} \end{bmatrix} = \begin{bmatrix} q_{ix}^{abs} + x_{OU} \\ q_{iy}^{abs} + y_{OU} \\ q_{iz}^{abs} + z_{OU} \end{bmatrix} = T_U^{abs} \begin{bmatrix} P_{ix}^U \\ P_{iy}^U \\ P_{iz}^U \end{bmatrix} \tag{10}$$

$$T_U^{abs} = \begin{bmatrix} R_B^{abs} & P_{OB}^{abs} \\ 0_{1\times 3} & 1 \end{bmatrix}$$

The final form of position vector for the lower connection point, could be derived considering that the transformation matrix of the lower platform is T_B^{abs}, as follows:

$$\vec{O}_i^{abs} = \begin{bmatrix} O_{ix}^{abs} \\ O_{iy}^{abs} \\ O_{iz}^{abs} \end{bmatrix} = \begin{bmatrix} S_{ix}^{abs} + x_{OB} \\ S_{iy}^{abs} + y_{OB} \\ S_{iz}^{abs} + z_{OB} \end{bmatrix} = T_U^{abs} \begin{bmatrix} O_{ix}^U \\ O_{iy}^U \\ O_{iz}^U \end{bmatrix} \tag{11}$$

$$T_B^{abs} = \begin{bmatrix} R_B^{abs} & P_{OB}^{abs} \\ 0_{1\times 3} & 1 \end{bmatrix}$$

The ith leg length (Euclidean distance) l_i and travel displacement of each linear actuator D_i, could be derived as follows:

$$\begin{aligned} l_i &= \left\| \vec{r}_i \right\| \\ D_i &= \delta l_i \end{aligned} \tag{12}$$

3.2 Leg unit vector

It is known that; the unit vector has the same direction as position vector. It is usually used to describe the orientation or direction in which the leg or linear actuator is pointing. The ith unit vector with respect to the absolute frame $\hat{e}_i$, could be derived considering that unit vector with respect to ith local frame is $\hat{e}_i^{f_i}$, as follows:

$$\begin{aligned} \hat{e}_i &= \frac{\vec{r}_i}{l_i} \\ \hat{e}_i &= R_{f_i}^{abs}\hat{e}_i^{f_i} \\ \hat{e}_i^{f_i} &= \begin{bmatrix} 0 & 0 & 1 \end{bmatrix}^T \end{aligned} \tag{13}$$

From equations 9 and 13, the ith leg unit vector, could be formulated as follows:

$$\hat{e}_i = \begin{bmatrix} e_{ix} \\ e_{iy} \\ e_{iz} \end{bmatrix} = \begin{bmatrix} C(\alpha_{Bi})S(\gamma_i) + S(\alpha_{Bi})S(\psi_i)C(\gamma_i) \\ C(\alpha_{Bi})S(\gamma_i) - C(\alpha_{Bi})S(\psi_i)C(\gamma_i) \\ C(\psi_i)C(\gamma_i) \end{bmatrix} \tag{14}$$

3.3 Velocity and acceleration analysis

For the upper platform, the velocity of tip connection P_i relative to the absolute frame $\vec{V}_{P_i}^{abs}$, could be derived considering that the velocity of the upper platform centre with respect to the absolute frame is $\vec{V}_{OU}^{abs}$, the velocity of point P_i relative to the upper platform centre with respect to the absolute frame is $\vec{V}_{P_i/OU}$, the upper platform angular velocity with respect to the absolute frame is $\vec{\omega}_{OU}^{abs}$, as follows:

$$\begin{aligned}
&\vec{V}_{P_i}^{abs} = \vec{V}_{OU}^{abs} + \vec{V}_{P_i/OU} \\
&\vec{V}_{OU}^{abs} = \vec{P}_{OU}^{abs} = \begin{bmatrix} \dot{x}_{OU} \\ \dot{y}_{OU} \\ \dot{z}_{OU} \end{bmatrix} \\
&\vec{V}_{P_i/OU} = \vec{\omega}_{OU}^{abs} \times \vec{q}_i^{abs}
\end{aligned} \tag{15}$$

Upper platform angular velocity with respect to the absolute frame, could be derived through Cardan's orientation order defined with respect to absolute frame as shown in (Fig. 5), considering that the unit vectors of the upper platform are $\hat{e}_{OUx}, \hat{e}_{OUy}, \hat{e}_{OUz}$ in [x_2–y_2–z_2] directions, respectively.

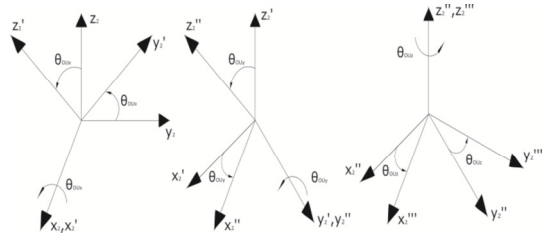

Figure 5. Upper platform Cardan's rotations

The upper platform angular velocity, could be derived considering that matrix associated with upper platform angular velocity is R_U, as follows:

$$\begin{aligned}
&\vec{\omega}_{OU}^{abs} = R_U \dot{\theta}_{OU} \\
&R_U = \begin{bmatrix} 1 & 0 & S(\theta_{OUy}) \\ 0 & C(\theta_{OUx}) & -S(\theta_{OUx})C(\theta_{OUy}) \\ 0 & S(\theta_{OUx}) & C(\theta_{OUx})C(\theta_{OUy}) \end{bmatrix}
\end{aligned} \tag{16}$$

The velocity of point P_i for the six actuators tip $V_{P_i}^{abs}$, could be written considering that velocity mapping from the upper platform centre to the ith leg connection with the upper platform relative to the absolute frame is $\dot{q}_U$, matrix associated with velocity mapping for the upper platform is J_1, as follows:

$$V_{P_i}^{abs} = J_1 \dot{q}_U \tag{17}$$

The acceleration of the six actuators tip $a_{P_i}^{abs}$, is derived considering that first derivative of its velocity mapping with respect to time is $\ddot{q}_U$, first derivative of the matrix associated with its velocity mapping with respect to time is $\dot{J}_1$, as follows:

$$\begin{aligned}
&a_{P_i}^{abs} = \frac{dV_{P_i}^{abs}}{dt} \\
&a_{P_i}^{abs} = \dot{J}_1 \dot{q}_U + J_1 \ddot{q}_U
\end{aligned} \tag{18}$$

The matrix associated with velocity mapping for the upper platform and its derivative with respect to time, are illustrated as follows:

$$\begin{aligned}
&J_1 = \begin{bmatrix} I_{3\times3} & -\vec{q}_i^{abs} \end{bmatrix} \\
&\dot{J}_1 = \begin{bmatrix} 0_{3\times3} & -\left(\vec{\omega}_{OU}^{abs} \times \vec{q}_i^{abs}\right) \end{bmatrix}
\end{aligned} \tag{19}$$

The velocity mapping of upper platform and its derivative with respect to time, could be derived considering that angular acceleration of the upper platform with respect to the absolute frame is α_{OU}^{abs}, the acceleration of the upper platform centre with respect to the absolute frame is a_{OU}^{abs}, as follows:

$$\begin{aligned}
&\dot{q}_U = \begin{bmatrix} V_{OU}^{abs} \\ \omega_{OU}^{abs} \end{bmatrix} \\
&\ddot{q}_U = \begin{bmatrix} a_{OU}^{abs} \\ \alpha_{OU}^{abs} \end{bmatrix}
\end{aligned} \tag{20}$$

The angular acceleration of the upper platform with respect to the absolute frame and the acceleration of the upper platform centre, could be derived considering that the first derivative of the matrix associated with upper platform angular velocity with respect to time is $\dot{R}_U$, as follows:

$$\begin{aligned}
&\vec{\alpha}_{OU}^{abs} = \vec{\omega}_{OU}^{abs} = \dot{R}_U \dot{\theta}_{OU} + R_U \ddot{\theta}_{OU} \\
&\vec{a}_{OU}^{abs} = \ddot{\vec{P}}_{OU}^{abs} = \begin{bmatrix} \ddot{x}_{OU} \\ \ddot{y}_{OU} \\ \ddot{z}_{OU} \end{bmatrix}
\end{aligned} \tag{21}$$

For the lower platform, the velocity of tip bottom connection O_i relative to the absolute frame $\vec{V}_{O_i}^{abs}$, could be derived considering that the velocity of the lower platform centre with respect to the absolute frame is $\vec{V}_{OB}^{abs}$, the velocity of point O_i relative to the lower platform centre with respect to the absolute frame is $\vec{V}_{O_i/OB}$, the lower platform angular velocity with respect to the absolute frame is $\vec{\omega}_{OB}^{abs}$, as follows:

$$\begin{aligned}
&\vec{V}_{O_i}^{abs} = \vec{V}_{OB}^{abs} + \vec{V}_{O_i/OB} \\
&\vec{V}_{OB}^{abs} = \vec{P}_{OB}^{abs} = \begin{bmatrix} \dot{x}_{OB} \\ \dot{y}_{OB} \\ \dot{z}_{OB} \end{bmatrix} \\
&\vec{V}_{O_i/OB} = \vec{\omega}_{OB}^{abs} \times \vec{S}_i^{abs}
\end{aligned} \tag{22}$$

Lower platform angular velocity with respect to the absolute frame, could be derived through Cardan's orientation order defined with respect to absolute frame as shown in (Fig. 6), considering that the unit vectors of the lower platform are $\hat{e}_{OUx}, \hat{e}_{OUy}, \hat{e}_{OUz}$ in [x1–y1–z1] directions respectively.

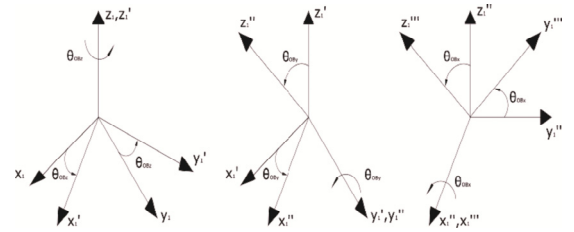

Figure 6. Lower platform Cardan's rotations

The lower platform angular velocity, could be derived considering that matrix associated with lower platform angular velocity is R_B, as follows:

$$\begin{aligned}
&\vec{\omega}_B^{abs} = R_B \dot{\theta}_{OB} \\
&R_B = \begin{bmatrix} C(O_{Bz})C(OBy) & -S(O_{Bz}) & 0 \\ S(O_{Bz})C(OBy) & C(O_{Bz}) & 0 \\ -S(Oy) & 0 & 1 \end{bmatrix} \\
&\dot{\theta}_i = \begin{bmatrix} \dot{\psi}_i \\ \dot{\gamma}_i \\ 0 \end{bmatrix}
\end{aligned} \tag{23}$$

The velocity of point O_i for the six actuators bottom $V_{O_i}^{abs}$, could be written considering that velocity map–ping from the lower platform centre to the ith leg connection with the lower platform relative to the abso–lute frame is $\dot{q}_B$, matrix associated with velocity mapping for the upper platform is J_2, as follows:

$$V_{O_i}^{abs} \tag{24}$$

The acceleration of the six actuators bottom $\alpha_{O_i}^{abs}$, is derived considering that first derivative of its velocity mapping with respect to time is $\ddot{q}_B$, first derivative of the matrix associated with its velocity mapping with respect to time is $\dot{J}_2$, as follows:

$$\begin{aligned}
&\alpha_{O_i}^{abs} = \frac{dV_{O_i}^{abs}}{dt} \\
&a_{O_i}^{abs} = \dot{J}_2 \dot{q}_B + J_2 \ddot{q}_B
\end{aligned} \tag{25}$$

The matrix associated with velocity mapping for the lower platform and its derivative with respect to time, are illustrated as follows:

$$\begin{aligned}
&J_2 = \begin{bmatrix} I_{3\times 3} & -\vec{S}_i^{abs} \end{bmatrix} \\
&\dot{J}_2 = \begin{bmatrix} 0_{3\times 3} & -\left(\vec{\omega}_{OU}^{abs} \times \vec{S}_i^{abs}\right) \end{bmatrix}
\end{aligned} \tag{26}$$

The velocity mapping of lower platform and its derivative with respect to time, could be derived consi–dering that angular acceleration of the lower platform with respect to the absolute frame is $\hat{e}_{ix}, \hat{e}_{iy}, \hat{e}_{iz}$, the acceleration of the lower platform centre with respect to the absolute frame is α_{OB}^{abs}, as follows:

$$\begin{aligned}
&\dot{q}_B = \begin{bmatrix} V_{OB}^{abs} \\ \omega_{OB}^{abs} \end{bmatrix} \\
&\ddot{q}_B = \begin{bmatrix} a_{OB}^{abs} \\ \alpha_{OB}^{abs} \end{bmatrix}
\end{aligned} \tag{27}$$

The angular acceleration of the lower platform with respect to the absolute frame and the acceleration of the lower platform centre, could be derived considering that the first derivative of the matrix associated with lower platform angular velocity with respect to time is $\dot{R}_B$, as follows:

$$\begin{aligned}
&\alpha_{OB}^{abs} = \vec{\omega}_{OB}^{abs} = \dot{R}_B \dot{\theta}_{OB} + R_B \ddot{\theta}_{OB} \\
&\vec{a}_{OB}^{abs} = \ddot{\vec{P}}_{OB}^{abs} = \begin{bmatrix} \ddot{x}_{OB} \\ \ddot{y}_{OB} \\ \ddot{z}_{OB} \end{bmatrix}
\end{aligned} \tag{28}$$

For each linear actuator, the magnitudes of the linear actuator travel velocity v_i, could be derived, considering that the velocity vector of actuator tip P_i relative to the bottom O_i with respect to the absolute frame is $\vec{V}_{P_i/O_i}^{abs}$, as follows:

$$\begin{aligned}
&\vec{V}_{P_i}^{abs} = \vec{V}_{O_i}^{abs} + \vec{V}_{P_i/O_i}^{abs} \\
&\vec{V}_{P_i/O_i}^{abs} = \vec{V}_i^{abs} + \vec{\omega}_i^{abs} \times \vec{r}_i \\
&\vec{r}_i = l_i \hat{e}_i
\end{aligned} \tag{29}$$

Equation 29 could be more simplified and written as follows:

$$\vec{V}_{P_i}^{abs} = \vec{V}_{O_i}^{abs} + \vec{V}_i^{abs} + \vec{\omega}_i^{abs} \times \left(l_i \hat{e}_i\right) \tag{30}$$

The ith leg angular velocity $\vec{\omega}_i^{abs}$ could be derived through Cardan's orientation defined with respect to inertial space frame as shown in (Fig. 7).

By considering that the unit vectors of the ith are $\hat{e}_{ix}, \hat{e}_{iy}, \hat{e}_{iz}$ in $[x_{3i} - y_{3i} - z_{3i}]$ directions respectively, rotation angle about x_{3i} is ψ_i, rotation angle about y_{3i} is γ_i. The ith leg angular velocity, could be derived considering that matrix associated with lower platform angular velocity is R_i, as follows:

$$\begin{aligned}
&\vec{\omega}_i^{abs} = R_i \dot{\theta}_i \\
&R_i = \begin{bmatrix} C(\alpha_{Bi}) & -C(\psi_i)S(\alpha_{Bi}) & 0 \\ S(\alpha_{Bi}) & C(\psi_i)C(\alpha_{Bi}) & 0 \\ 0 & S(\psi_i) & 1 \end{bmatrix} \\
&\dot{\theta}_i = \begin{bmatrix} \dot{\psi}_i \\ \dot{\gamma}_i \\ 0 \end{bmatrix}
\end{aligned} \tag{31}$$

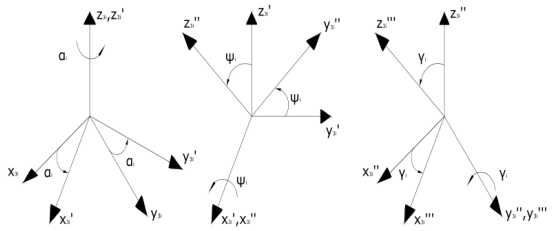

Figure 7. Cardan's rotations of ith leg

The speed of the six linear actuators V_i, could be determined from equation 30 as follows:

$$V_i = \hat{e}_i \odot \vec{V}_{P_i}^{abs} - \hat{e}_i \odot \vec{V}_{O_i}^{abs} \tag{32}$$

Linear actuator speed matrix for the six legs, could be derived considering that inverse Jacobian matrix of upper and lower platforms are J_U and J_B respectively, as follows:

$$\begin{aligned} V_i &= \begin{bmatrix} v_1 & v_2 & v_3 & v_4 & v_5 & v_6 \end{bmatrix}^T \\ &= J_U \dot{q}_U - J_B \dot{q}_B \end{aligned} \tag{33}$$

Type one and type two of the inverse Jacobian matrix associated with upper platform are J_{U1}, J_{U11} respectively, type one and type two of the inverse Jacobian matrix associated with lower platform are J_{B1}, J_{B11} respectively could be derived as follows:

$$\begin{aligned} J_U &= J_{U1} J_{U11} \\ J_B &= J_{B1} J_{B11} \end{aligned} \tag{34}$$

Type one of the inverse Jacobian matrices associated with the upper and lower platforms are typically the same as they are square 6×6 diagonal matrices. they could be derived as shown in the following equation.

$$J_{B1} = J_{U1} = \begin{bmatrix} \frac{1}{l_1} & 0 & 0 & 0 & 0 & 0 \\ 0 & \frac{1}{l_2} & 0 & 0 & 0 & 0 \\ 0 & 0 & \frac{1}{l_3} & 0 & 0 & 0 \\ 0 & 0 & 0 & \frac{1}{l_4} & 0 & 0 \\ 0 & 0 & 0 & 0 & \frac{1}{l_5} & 0 \\ 0 & 0 & 0 & 0 & 0 & \frac{1}{l_6} \end{bmatrix} \tag{35}$$

Type two of the inverse Jacobian matrix associated with the upper platform is 6×6 square matrix and could be derived as follows:

$$J_{U11} = \begin{bmatrix} \vec{r}_1^T & \left(\vec{q}_1^{abs} \times \vec{r}_1\right)^T \\ \vec{r}_2^T & \left(\vec{q}_2^{abs} \times \vec{r}_2\right)^T \\ \vec{r}_3^T & \left(\vec{q}_3^{abs} \times \vec{r}_3\right)^T \\ \vec{r}_4^T & \left(\vec{q}_4^{abs} \times \vec{r}_4\right)^T \\ \vec{r}_5^T & \left(\vec{q}_5^{abs} \times \vec{r}_5\right)^T \\ \vec{r}_6^T & \left(\vec{q}_6^{abs} \times \vec{r}_6\right)^T \end{bmatrix} \tag{36}$$

Type two of the inverse Jacobian matrix associated with the lower platform is 6×6 square matrix and could be derived as follows:

$$J_{B11} = \begin{bmatrix} \vec{r}_1^T & \left(\vec{S}_1^{abs} \times \vec{r}_1\right)^T \\ \vec{r}_2^T & \left(\vec{S}_2^{abs} \times \vec{r}_2\right)^T \\ \vec{r}_3^T & \left(\vec{S}_3^{abs} \times \vec{r}_3\right)^T \\ \vec{r}_4^T & \left(\vec{S}_4^{abs} \times \vec{r}_4\right)^T \\ \vec{r}_5^T & \left(\vec{S}_5^{abs} \times \vec{r}_5\right)^T \\ \vec{r}_6^T & \left(\vec{S}_6^{abs} \times \vec{r}_6\right)^T \end{bmatrix} \tag{37}$$

When the parallel manipulator loses or gains one or more degrees-of-freedom (DOF) at a definite position, then that position is defined as a singular position [25]. To avoid singularities, type two of the inverse Jacobian matrix associated with upper and lower platforms J_{UII} and J_{BII} respectively should have an inverse so that

$$\det\left(J_{U11}\right) \neq 0 \; \textit{and} \; \det\left(J_{B11}\right) \neq 0 \tag{38}$$

The acceleration matrix of the six linear actuators a_i, could be derived as follows:

$$\begin{aligned} a_i &= \begin{bmatrix} a_1 & a_2 & a_3 & a_4 & a_5 & a_6 \end{bmatrix}^T \\ &= \frac{dV_i}{dt} = \left[\dot{J}_U \dot{q}_U + J_U \ddot{q}_U\right] - \left[\dot{J}_B \dot{q}_B + J_B \ddot{q}_B\right] \end{aligned} \tag{39}$$

Considering that first derivative of the inverse Jacobian matrix associated with the upper platform with respect to time is $\dot{J}_U$ is derived as follows:

$$\dot{J}_U = \begin{bmatrix} \hat{e}_1^T & \left(\left(\vec{\omega}_{OU}^{abs} \times \vec{P}_1^{abs}\right) \times \hat{e}_1^T + \vec{P}_1^{abs}\right) \times \hat{e}_1)^T \\ \hat{e}_2^T & \left(\left(\vec{\omega}_{OU}^{abs} \times \vec{P}_2^{abs}\right) \times \hat{e}_2^T + \vec{P}_2^{abs}\right) \times \hat{e}_2)^T \\ \hat{e}_3^T & \left(\left(\vec{\omega}_{OU}^{abs} \times \vec{P}_3^{abs}\right) \times \hat{e}_3^T + \vec{P}_3^{abs}\right) \times \hat{e}_3)^T \\ \hat{e}_4^T & \left(\left(\vec{\omega}_{OU}^{abs} \times \vec{P}_4^{abs}\right) \times \hat{e}_4^T + \vec{P}_4^{abs}\right) \times \hat{e}_4)^T \\ \hat{e}_5^T & \left(\left(\vec{\omega}_{OU}^{abs} \times \vec{P}_5^{abs}\right) \times \hat{e}_5^T + \vec{P}_5^{abs}\right) \times \hat{e}_5)^T \\ \hat{e}_6^T & \left(\left(\vec{\omega}_{OU}^{abs} \times \vec{P}_6^{abs}\right) \times \hat{e}_6^T + \vec{P}_6^{abs}\right) \times \hat{e}_6)^T \end{bmatrix} \tag{40}$$

Considering that first derivative of the inverse Jacobian matrix associated with the lower platform with respect to time is $\dot{J}_B$ is derived as follows:

$$\dot{J}_B = \begin{bmatrix} \hat{e}_1^T & \left(\left(\vec{\omega}_{OB}^{abs} \times \vec{P}_1^{abs}\right) \times \hat{e}_1^T + \vec{O}_1^{abs}\right) \times \hat{e}_1)^T \\ \hat{e}_2^T & \left(\left(\vec{\omega}_{OB}^{abs} \times \vec{P}_2^{abs}\right) \times \hat{e}_2^T + \vec{O}_2^{abs}\right) \times \hat{e}_2)^T \\ \hat{e}_3^T & \left(\left(\vec{\omega}_{OB}^{abs} \times \vec{P}_3^{abs}\right) \times \hat{e}_3^T + \vec{O}_3^{abs}\right) \times \hat{e}_3)^T \\ \hat{e}_4^T & \left(\left(\vec{\omega}_{OB}^{abs} \times \vec{P}_4^{abs}\right) \times \hat{e}_4^T + \vec{O}_4^{abs}\right) \times \hat{e}_4)^T \\ \hat{e}_5^T & \left(\left(\vec{\omega}_{OB}^{abs} \times \vec{P}_5^{abs}\right) \times \hat{e}_5^T + \vec{O}_5^{abs}\right) \times \hat{e}_5)^T \\ \hat{e}_6^T & \left(\left(\vec{\omega}_{OB}^{abs} \times \vec{P}_6^{abs}\right) \times \hat{e}_6^T + \vec{O}_6^{abs}\right) \times \hat{e}_6)^T \end{bmatrix} \tag{41}$$

3.4 Leg rotation angles

The rotation angles of the universal joint of ith leg, could be derived in terms of the components of direc–tion cosines (unit vectors) of each leg while considering the upper and lower platform generalized coordinates, transformation matrices of both upper and lower platforms and leg length, as follows:

$$\hat{e}_i = \begin{bmatrix} e_{ix} \\ e_{iy} \\ e_{iz} \end{bmatrix} = \frac{T_U^{abs}\vec{P}_i^U - T_B^{abs}\vec{P}_i^B}{l_i} \tag{42}$$

$$\begin{aligned} e_{ix} &= \frac{1}{l_i}\left[T_{U_{1\times(1-4)}}P_i^U - T_{B_{1\times(1-4)}}O_i^B\right] \\ e_{iy} &= \frac{1}{l_i}\left[T_{U_{2\times(1-4)}}P_i^U - T_{B_{2\times(1-4)}}O_i^B\right] \\ e_{iz} &= \frac{1}{l_i}\left[T_{U_{3\times(1-4)}}P_i^U - T_{B_{3\times(1-4)}}O_i^B\right] \end{aligned} \tag{43}$$

The first derivative of ith leg direction cosines $\dot{e}_{ix}, \dot{e}_{iy}$ and $\dot{e}_{iz}$ with respect to time, could be derived considering that first derivative of the transformation matrix with respect to time of upper platform is $\dot{T}_B^{abs}$ and first derivative of the transformation matrix with respect to time of lower platform is $\dot{T}_B^{abs}$, as follows:

$$\begin{aligned} \dot{e}_{ix} &= \frac{\dot{T}_{u_{1\times(1-4)}}P_i^U - \dot{T}_{B_{1\times(1-4)}}O_i^B - e_{ix}v_i}{l_i} \\ \dot{e}_{iy} &= \frac{\dot{T}_{u_{2\times(1-4)}}P_i^U - \dot{T}_{B_{2\times(1-4)}}O_i^B - e_{iy}v_i}{l_i} \\ \dot{e}_{ix} &= \frac{\dot{T}_{u_{3\times(1-4)}}P_i^U - \dot{T}_{B_{3\times(1-4)}}O_i^B - e_{iz}v_i}{l_i} \end{aligned} \tag{44}$$

The second derivative of ith leg direction cosines $\ddot{e}_{ix}, \ddot{e}_{iy}$ and $\ddot{e}_{iz}$ with respect to time, could be derived considering that second derivative of the transformation matrix with respect to time of upper platform is $\ddot{T}_U^{abs}$ and second derivative of the transformation matrix with respect to time of lower platform is $\ddot{T}_B^{abs}$, as follows:

$$\begin{aligned} \ddot{e}_{ix} &= \frac{\ddot{T}_{u_{1\times(1-4)}}P_i^U - \ddot{T}_{B_{1\times(1-4)}}O_i^B - 2\dot{e}_{ix}v_i - e_{ix}a_i}{l_i} \\ \ddot{e}_{iy} &= \frac{\ddot{T}_{u_{2\times(1-4)}}P_i^U - \ddot{T}_{B_{2\times(1-4)}}O_i^B - 2\dot{e}_{iy}v_i - e_{iy}a_i}{l_i} \\ \ddot{e}_{ix} &= \frac{\ddot{T}_{u_{3\times(1-4)}}P_i^U - \ddot{T}_{B_{3\times(1-4)}}O_i^B - 2\dot{e}_{iz}v_i - e_{iz}a_i}{l_i} \end{aligned} \tag{45}$$

From equations 14 and 43 the ith leg rotation angles in terms of generalized coordinates are derived as follows:

$$\begin{aligned} e_{ix} &= C(\alpha_{Bi})S(\gamma_i) + S(\alpha_{Bi})S(\psi_i)C(\gamma_i) \\ e_{iy} &= S(\alpha_{Bi})S(\gamma_i) - C(\alpha_{Bi})S(\psi_i)C(\gamma_i) \\ e_{iz} &= C(\psi_i)C(\gamma_i) \end{aligned} \tag{46}$$

The rotation angle about y_{3i}, its first derivative with respect to time $\dot{\gamma}_i$ and its second derivative with respect to time $\ddot{\gamma}_i$ could be derived as follows:

$$C(\alpha_{Bi})e_{ix} + S(\alpha_{Bi})e_{iy} = S(\gamma_i) \tag{47}$$

$$\begin{aligned} \gamma_i &= S^{-1}\left(C(\alpha_{Bi})e_{ix} + S(\alpha_{Bi})e_{iy}\right) \\ \dot{\gamma}_i &= \frac{C(\alpha_{Bi})\dot{e}_{ix} + S(\alpha_{Bi})\dot{e}_{iy}}{C(\gamma_i)} \\ \ddot{\gamma}_i &= \frac{C(\alpha_{Bi})\ddot{e}_{ix} + S(\alpha_{Bi})\ddot{e}_{iy} + \dot{\gamma}_i S(\gamma_i)}{C(\gamma_i)} \end{aligned} \tag{48}$$

From equation 46 the rotation angle about x_{3i}, its first derivative with respect to time ψ_i and its second derivative with respect to time $\ddot{\psi}_i$ could be derived as follows:

$$S(\alpha_{Bi})e_{ix} - C(\alpha_{Bi})e_{iy} = S(\psi_i)C(\gamma_i) \tag{49}$$

$$\begin{aligned} \dot{\psi}_i &= \left(\frac{S(\alpha_{Bi})\dot{e}_{ix} - C(\alpha_{Bi})\dot{e}_{iy} - \tan(\psi_i)e_{iz}}{e_{iz}}\right)C^2(\psi_i) \\ \ddot{\psi}_i &= \left(\frac{S(\alpha_{Bi})\ddot{e}_{ix} - C(\alpha_{Bi})\ddot{e}_{iy}}{e_{iz}}\right)C^2(\psi_i) \\ &+ \left(\frac{-2\psi_i \sec^2(\psi_i)\tan(\psi_i)e_{iz}}{e_{iz}}\right)C^2(\psi_i) \\ &+ \left(\frac{-2\psi_i \sec^2(\psi_i)\ddot{e}_{iz} - \tan(\psi_i)\ddot{e}_{iz}}{e_{iz}}\right)C^2(\psi_i) \end{aligned} \tag{50}$$

The derived inverse kinematic model is the foun–dation for understanding and directing the motion of the Stewart platform. It gives a mathematical foundation for precisely computing system positions, velocities and accelerations. This model could be used to create precise control algorithms, optimize performance, and mimic the platform's behavior in a variety of circum–stances. It is crucial for bridging the gap between theory and practice, allowing the platform to do complicated tasks with precision and efficiency.

4. MODELING OF STEWART PLATFORM

In order to fully understand the Stewart platform's compli–cated motion patterns, this section reveals the basic prin–ciples that control the movement of platform using the pre–viously derived kinematic mathematical model and thoro–ugh analysis, providing insights into its motion capabilities. It presents an extensive kinematic model that explains how joint angles and actuator lengths relate to the position and orientation of the platform in space. The platform's flexibility and ability to accomplish exact positioning will be easily visualized thanks to this model.

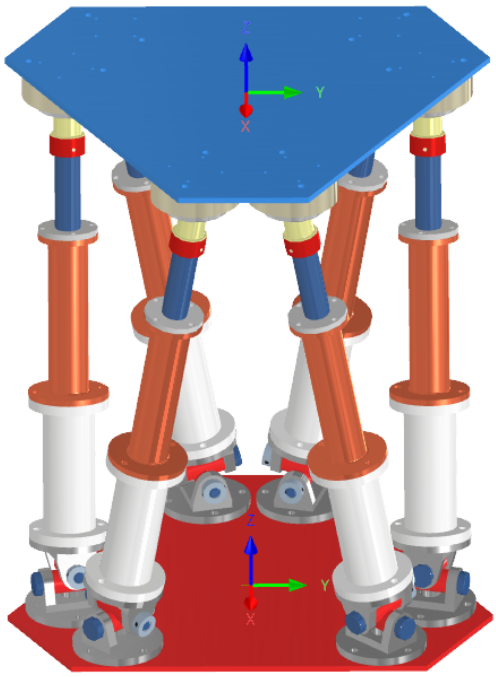

Figure 8. Designed Stewart platform

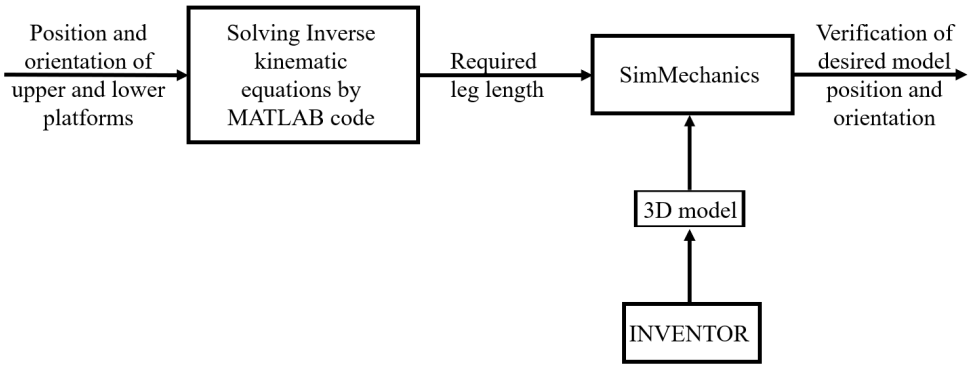

Figure 9. Simulation analysis

The kinematic mathematical model has two inputs represented in position and orientation of both upper and lower platforms as a function of time. The 3D model has been designed using INVENTOR, as shown in (Fig. 8), according to the parameters shown in table 1.

Table 1. Values of design parameters

Parameter	Value
r	184 mm
i	[1,2,3,4,5,6]
α_{Ui}	[15°,105°,135°,225°,255°,345°]
α_{Bi}	[45°,75°,165°,195°,285°,315°]

The designed Stewart platform's 3D model was directly integrated into SimMechanics, setting the way for the conversion of theoretical equations into usable code. The derived kinematic model was coded in MATLAB. The model solution on MATLAB generates lengths, speeds, accelerations and rotation angles of each leg. The solution of kinematic problem is verified with the aid of INVENTOR, MATLAB and SimMechanics, as shown in (Fig. 9)

4.1 Workspace analysis

The model constrains, degrees of freedom of joints and frames should be assigned to facilitate simulation and analysis. The Stewart platform's angle limits specify the acceptable range of motion for each joint. These restrictions are put into consideration to make sure that moving the platform is still physically possible and secure. Angle limitations are essential for avoiding scenarios in which joints are moved to extreme angles that can cause mechanical interference, overload actuators, or other unfavorable effects. The designed universal joint is permitting rotation about its two perpendicular axes from −32.25° to 32.25°, while the designed spherical joint is permitting tilt angle about its perpendicular axis up to 24.25° and the designed actuator is permitting stroke length to vary from 0 mm up to 150 mm.

These constrains serve to precisely specify the possible range of movements of each leg in a specific region of space. The workspace of a leg with a linear actuator and a universal joint at its base is a complicated geometric volume in three dimensions. The permissible maximum and minimum angles of joints, the length

restrictions for linear actuator extensions and any mechanical interference that might happen while the leg is moving all have an impact on this volume. Since each leg contains spherical joints at the top and universal joints at the bottom, angle limitations are minimized to the smallest limit of both joints, as follows:

$$\begin{aligned} D_i &= [0:150]mm \\ \gamma_i &= [-24.25°:24.25°] \\ \psi_i &= [-24.25°:24.25°] \end{aligned} \tag{51}$$

As shown in (Fig. 10) the upper platform has a vertical displacement range starts from 415.705 mm to 568.565 mm, defined by a plan parallel to the upper platform top surface with 31 mm shift down in z direction and containing all centres of spherical joints. Similarly, the range is measured from a plan parallel to the lower platform top surface with 31 mm shift up in z direction and containing all centres of lower cylinders of universal joints, these plans are called upper and lower platforms plans respectively.

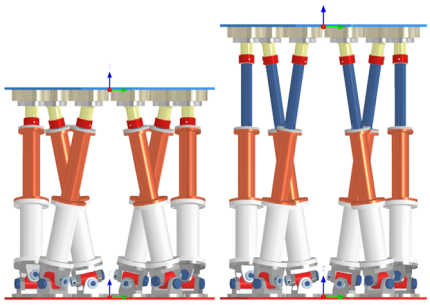

Figure 10. Vertical range spanned by the upper platform

The workspace of each leg is customized to fit within the constraints set by the upper platform vertical range. This interaction makes sure that the mobility of the legs is in perfect harmony with the limits of the upper platform. As shown in (Fig. 11) and (Fig. 12).

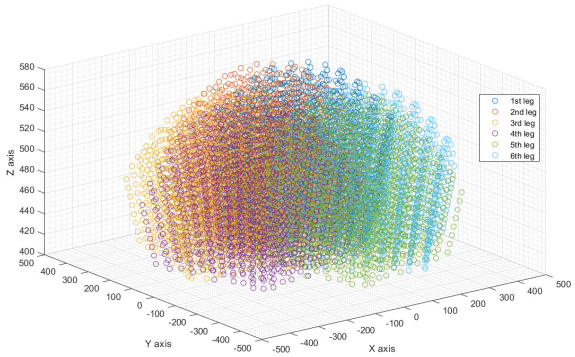

Figure 11. 3D workspace of Stewart platform legs

The intersection region of the six workspaces of the linear actuators can give specific indication to the overall platform workspace. This planned workspace is not only mechanically necessary, but also a crucial element in the platform's efficiency. It guarantees that the end-effector of the platform can be positioned precisely in the area where all legs can manipulate together. The use of this collabo–rative workspace facilitates complex motions and improves the platform's ability for synchronized interac–tion with objects or environment.

4.2 Numerical and simulation analysis

The SimMechanics model simulates the physical behavior of the Stewart platform and acts as its digital twin. It provides a real-time simulation analysis to forecast and visualize the platform's motion, responses to different inputs and interactions. Mechanical parts and connections are represented by blocks that are assembled to build the model. As shown in (Fig. 13), the driving inputs for the prismatic joints in the SimMechanics environment are the values determined for the leg lengths in MATLAB.

The movement of the platform can be simulated due to the integration between MATLAB and SimMechanics. The lengths are translated into the extension and retraction of the prismatic joints.

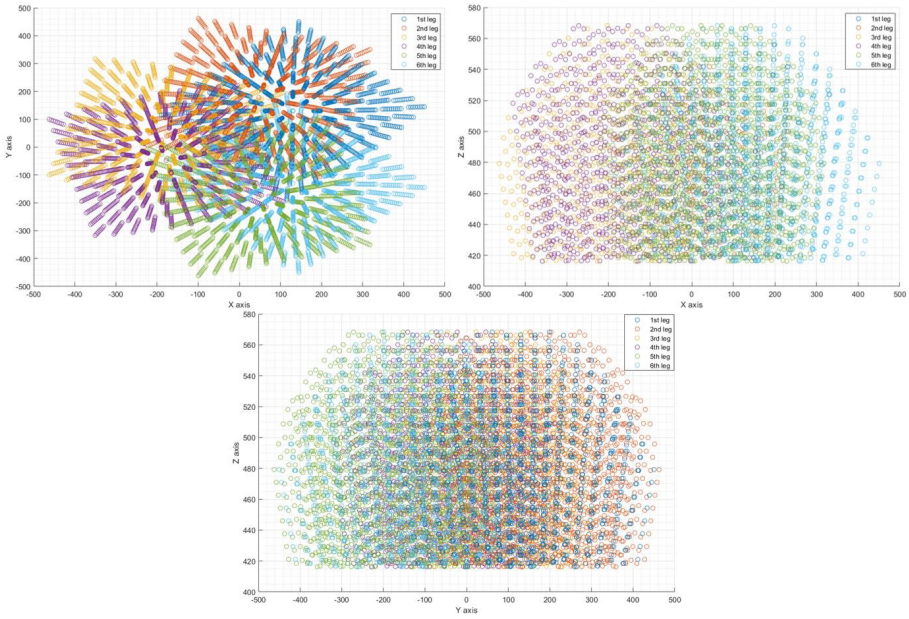

Figure 12. 2D workspace of Stewart platform legs

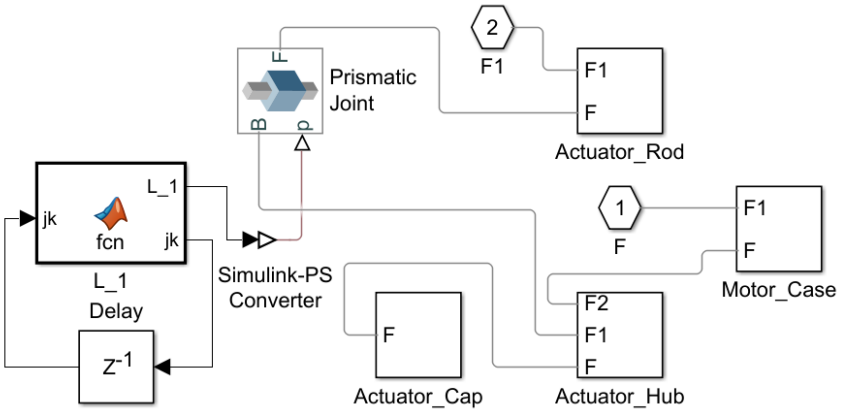

Figure 13. Block diagram of linear actuator

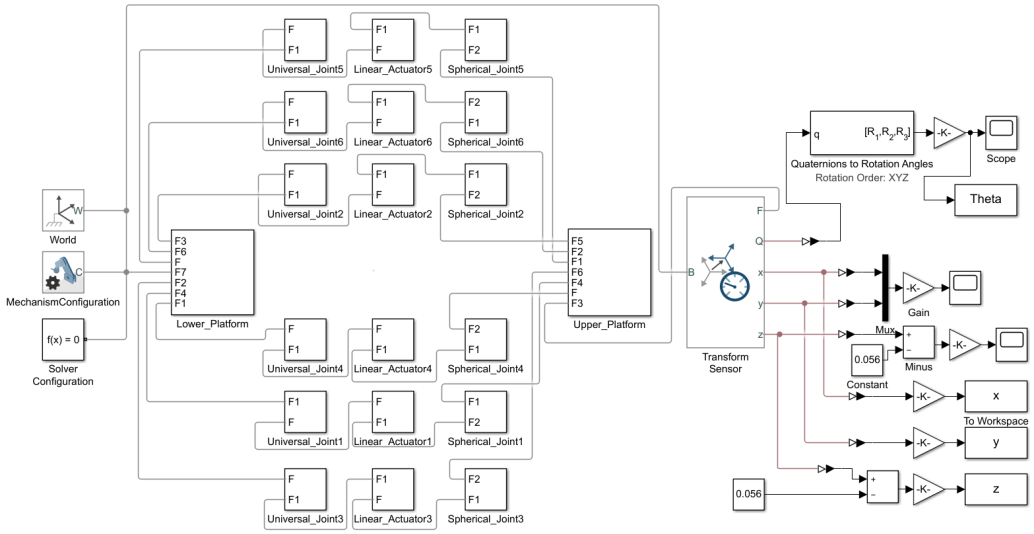

Figure 14. Block diagram of Stewart platform

As shown in (Fig. 14), the block diagram representing the Stewart model built in SimMechanics.

There will be two different path tracking scenarios. The first considers obeying the upper platform to a definite path while the lower platform is moving. The other considers obeying the upper platform to a definite path while the lower platform is kept stationary.

4.3 First path tracking scenario

The goal of this scenario is to make sure that the platform follows the desired path while legs lengths, velocities, accelerations and rotation angles are within their ranges. The scenario has been simulated as illustrated in the following equation, considering that simulation time t is measured in (seconds) and all position coordinates are measured in mm.

$$\vec{P}_{OB}^{abs} = \begin{bmatrix} 0.4t & -0.2t & -3\cos(\pi t) \end{bmatrix}^T$$
$$\theta_{OB} = \begin{bmatrix} 0.3°t & 0.3°t & 0.2°t \end{bmatrix}^T \quad (52)$$

$$\vec{P}_{OU}^{abs} = \begin{bmatrix} 4.5\cos(\pi t) & 4.5\sin(\pi t) & 11.5t + 415.706 \end{bmatrix}^T$$
$$\theta_{OU} = \begin{bmatrix} 0.5°t & 1°t & 1.5°t \end{bmatrix}^T \quad (53)$$

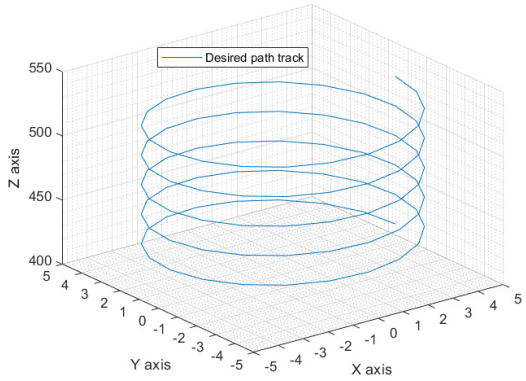

Figure 15. Desired path of first scenario of upper platform plan centre

In (Fig. 15), the depicted path illustrates the optimal trajectory for the centre of the upper platform. This ideal path signifies the desired movement or position that the upper platform should follow. It's crucial to note that in this tracking scenario, there's additional complexity introduced by the movement of the lower platform. This interplay between the upper and lower platforms adds a layer of intricacy to the tracking process, requiring precise coordination and control to ensure the upper

platform stays aligned with its intended path despite the dynamic movement of the lower platform.

As shown in (Fig. 16), lengths of legs of the Stewart platform vary over time but it hadn't exceeded the maximum value of actuator stroke. It consists of one or more lines, each corresponding to the length of a single leg and spanning a ten seconds time period.

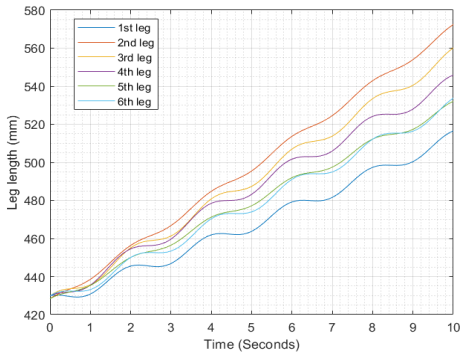

Figure 16. Variation of legs lengths in the first scenario

Legs linear velocity, as shown in (Fig. 17), reflects the rate at which the platform's individual legs extend or retract over time. Velocity indicates how rapidly the platform's legs are adjusting during scenario.

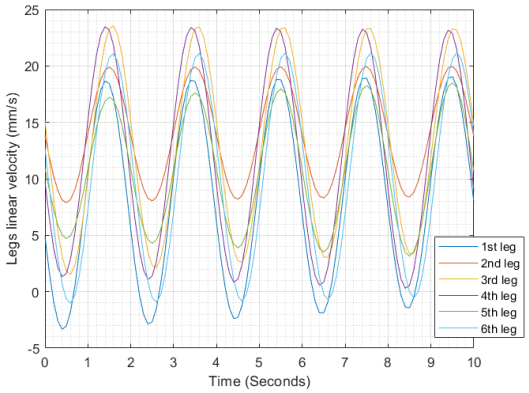

Figure 17. Variation of legs velocities in the first scenario

Legs linear acceleration, shown in (Fig. 18), shows how rapidly the platform's individual legs change their extension or retraction rates over time.

Acceleration data is critical for understanding how the platform's legs respond to external forces or control inputs dynamically.

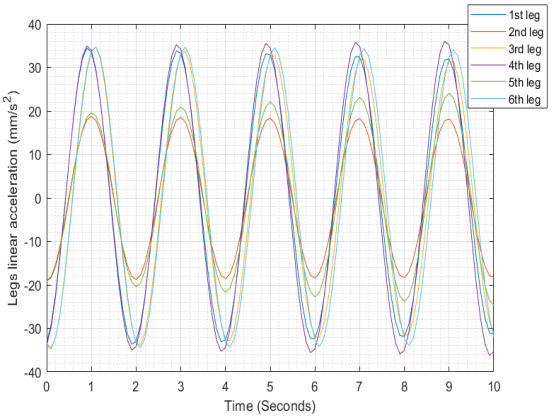

Figure 18. Variation of legs accelerations in the first scenario

Universal joint rotation angles, as represented in the (Fig. 19), show the angular shifts measured in degrees that occur about the two axes of universal joints over time, which is crucial for properly and effectively positioning the platform.

It is clear that the rotation angles hadn't exceeded the joint constraints.

As shown in (Fig. 20), the simulation in MATLAB concludes with the determination of the final position and orientation of both the upper and lower plans of the platforms at the end of the simulation time.

When the simulation is finished, it provides an exact snapshot of where each platform is positioned and how it is orientated.

These final locations and orientations are critical for evaluating the platform's performance, confirming design decisions, and ensuring that it matches with the simulation's intended objectives.

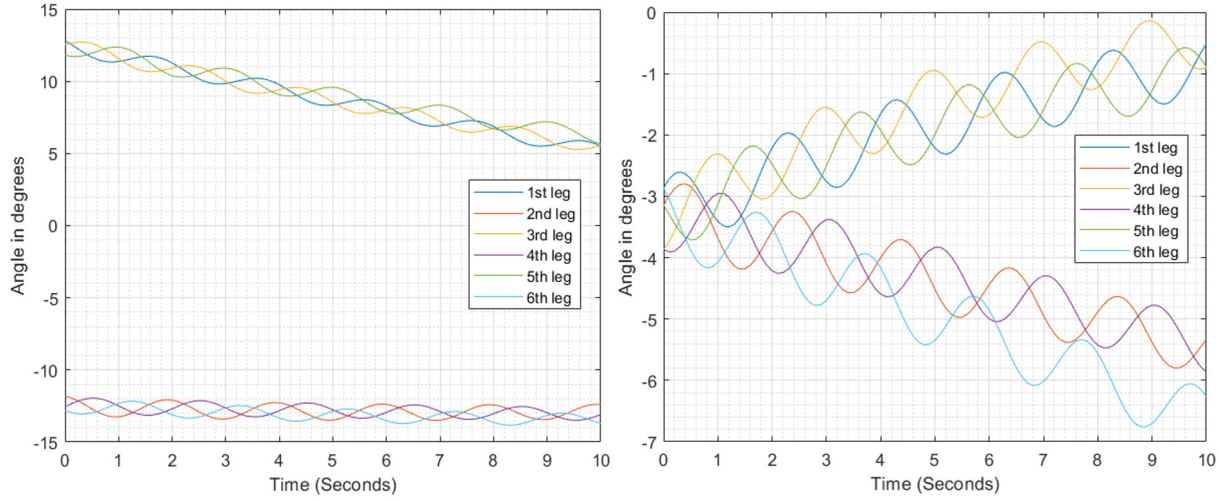

Figure 19. Variation of legs angles (ψ_i on left and γ_i on right) in the first scenario

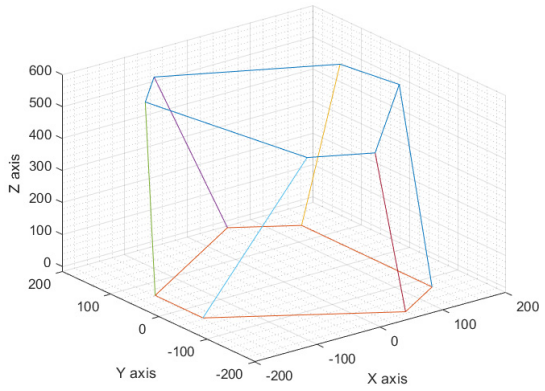

Figure 20. Position and orientation of the platform plans at the end of first scenario

4.4 Second path tracking scenario

In the second path tracking scenario. Here, the lower platform is immobile while the upper platform dutifully follows a predetermined trajectory. The lower platform frame coincides with the inertial frame. The upper platform navigates its 3D span while the lower platform acts as a steady base in this simulation scenario as follows:

$$\vec{P}_{OB}^{abs} = \begin{bmatrix} 0 & 0 & 0 \end{bmatrix}^T \qquad \theta_{OB} = \begin{bmatrix} 0 & 0 & 0 \end{bmatrix}^T \tag{54}$$

$$\vec{P}_{OU}^{abs} = \begin{bmatrix} 5t & 0.5\sin(\pi t) & 8t + 415.706 \end{bmatrix}^T \qquad \theta_{OU} = \begin{bmatrix} 0.5°t & 1.25°t & 2°t \end{bmatrix}^T \tag{55}$$

The desired path shown in (Fig. 21), illustrates the path that centre of the upper platform plan should take during the second scenario.

In (Fig. 22), the depicted trajectory showcases the simulated position of the centre of the upper platform as obtained from the model simulation in SimMechanics. The simulation captures the movement of the upper platform in a three-dimensional space.

Notably, the right side of the figure represents the evolution of the z-coordinate, providing insights into the vertical movement of the centre of the upper platform. Meanwhile, on the left side, the x and y coordinates unfold, offering a comprehensive view of the horizontal displacement.

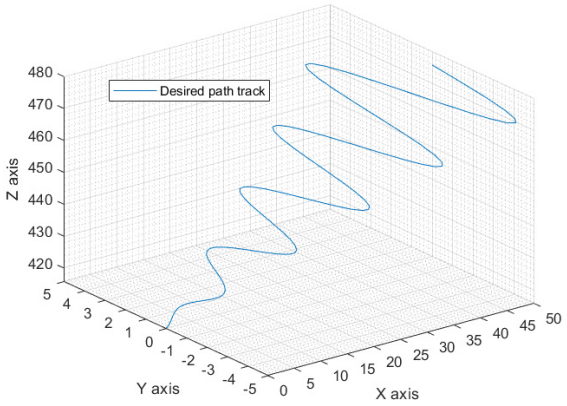

Figure 21. Desired path of second scenario of upper platform plan centre

As shown in (Fig. 23), the visualization presents a detailed representation of the orientation followed by the upper platform plan during second scenario.

As shown in (Fig. 24), the simulation in MATLAB concludes with the determination of the final position and orientation of both the upper and lower plans of the platforms at the end of the simulation time. As well, SimMechanics represents the final position and orientation of the platform at the end of second scenario.

As shown in (Fig. 25), the path track obtained by Simulink simulation provides a thorough illustration of the platform's motion as it moves along a predetermined path. The path track turns into a tool for assessing how closely the platform follows the intended route by contrasting the simulated path with the anticipated trajectory. Additionally, it makes it easier to assess the platform's overall performance by pointing out any flaws that might call for mechanical aspect upgrades. Beyond validation, the path track enables to mimic and examine the platform's responses in actual circumstances.

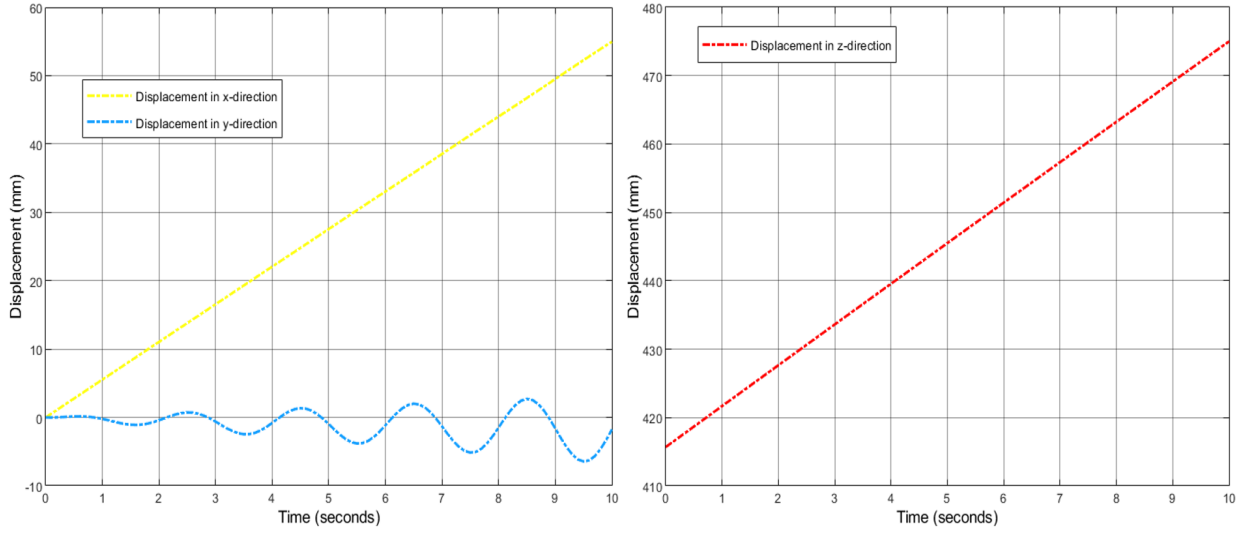

Figure 22. Position of centre of upper platform plan during second scenario

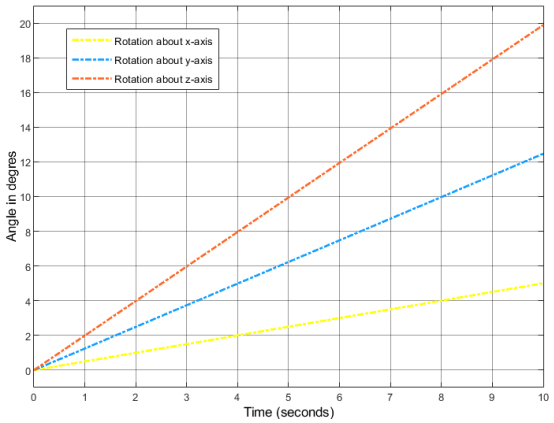

Figure 23. Orientation of the upper platform plan at the end of second scenario

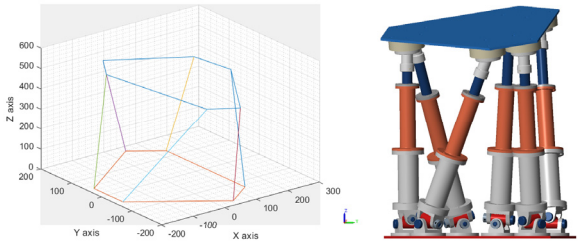

Figure 24. Position and orientation at the end of second scenario

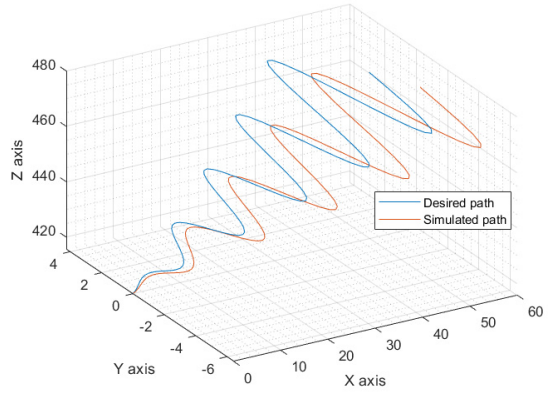

Figure 25. Comparison between desired and simulated path tracks of second scenario

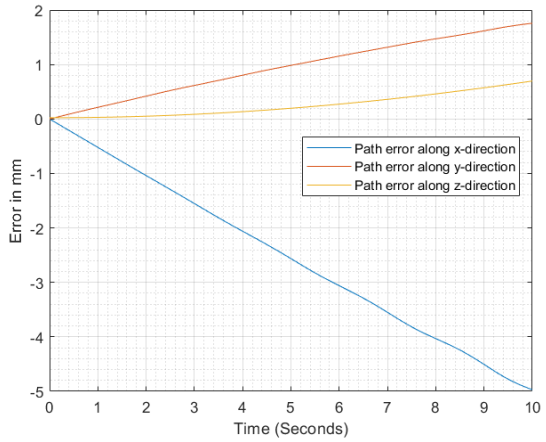

Figure 26. Path track error in 3D of second scenario

The path track error, as shown in (Fig. 26), offers an important evaluation of the platform motion. This inaccuracy measures the differences between the plat–form's real path and the simulated path along the X, Y, and Z axes. It is clear that, the error gradually and linearly increases over time, but it hadn't exceeded 10% about any axis.

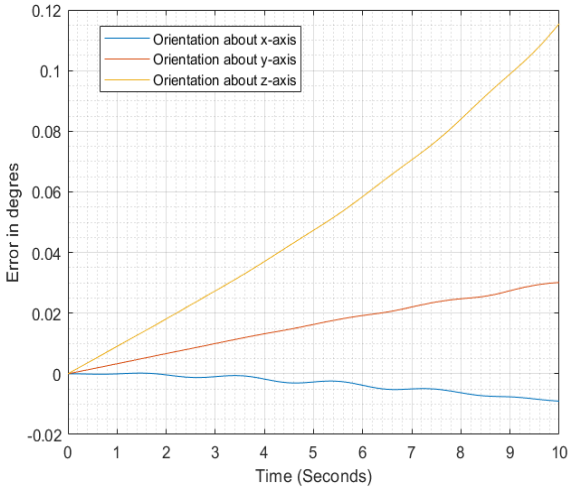

Figure 27. Orientation error of second scenario

5. STEWART PLATFORM EXPERIMENTAL MODEL

The experimental model of Stewart platform uses an Arduino Mega to create the control signal for Cytron MDD10A motor drivers, which controls the direction and positioning of the electric linear actuators. Ultrasonic sensors are deployed in parallel to track and measure the output displacements.

The control system is subsequently updated in real-time with these data, giving feedback on the precise measured displacement. The MPU6050 is utilized to track and measure the orientation of the upper platform. The scheme presented in (Fig. 30), provides a clear illustration of the wiring schematic for the Stewart platform, highlighting the connections between parts used in this control system design.

The difference between the desired and actual orientations of a platform is referred to as orientation error. It measures the degree to which the platform's orientation differs from its intended or desired orientation. When performing operations that require precise alignment or orientation, it is necessary to understand orientation inaccuracy.

As shown in (Fig. 27), the error about the X, Y, and Z axes. The effect of following very difficult path caused the error to linearly increase over time, but it hadn't exceeded 2.32% about any axis. The error in both position and orientation comes out from making the platform obeying very difficult path.

In this experimental model the used controller for linear actuators is the designed PID controller mentioned in M. R. Mohamed et al. [26].

The wiring of the designed Stewart platform experimental model and how the components are wired together is illustrated in (Fig. 29).

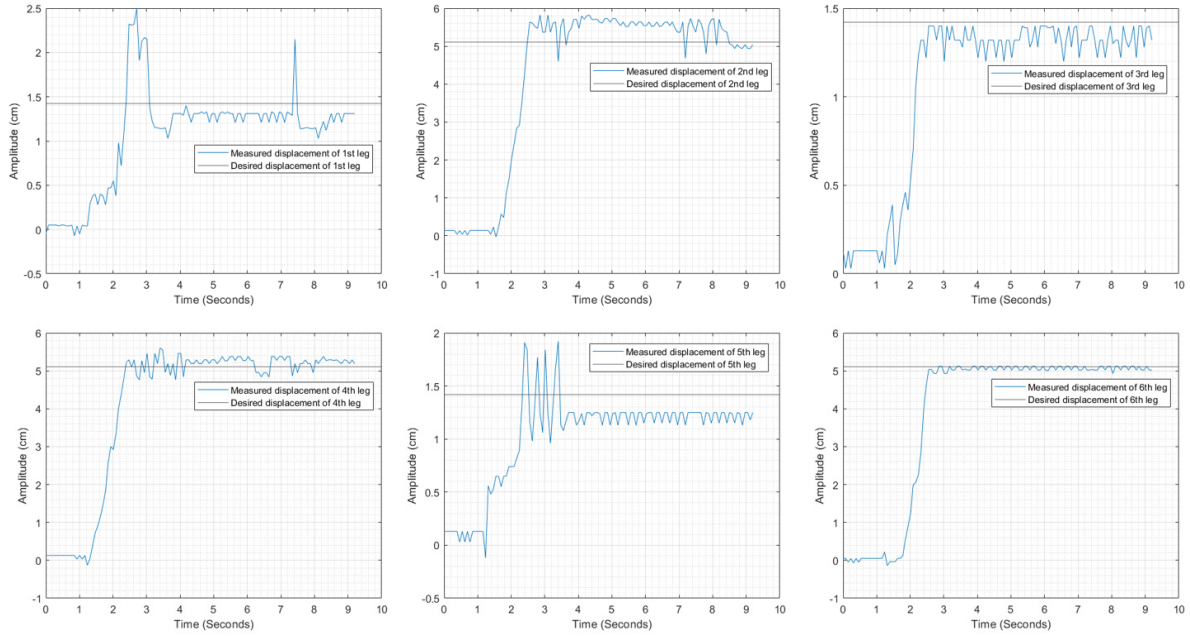

Figure 28. Electric linear actuators response to desired displacements in first experimental scenario

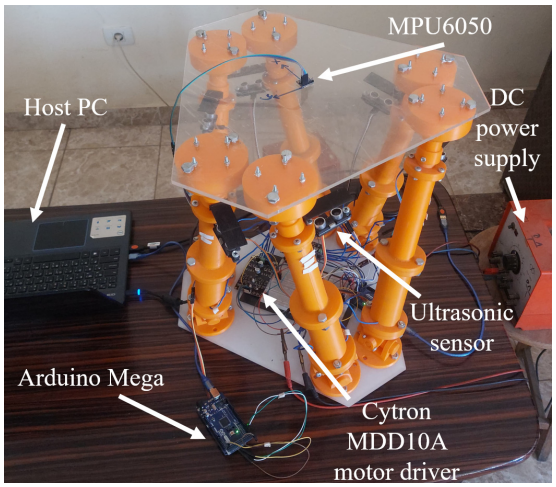

Figure 29. Stewart platform experimental model

5.1 Experimental tests

The upper platform must be at its zero or home position before starting any scenarios. The measuring procedure is carried out with a 1.2 second wait before the scenario begins, giving the sensors plenty of time to gather accurate data.

This preliminary information is crucial for monitoring leg motions and calculating length changes throughout various scenarios. While the lower platform is kept stationary, the kinematic mathematical model states that the position and orientation of the upper platform are inextricably linked to the displacements of the legs. Accurately achieving the location of the upper platform follows naturally from achieving the leg displacements and upper platform orientation. The scenario's precise positioning and motion control are built on this foundation. The two simulation scenarios are varied from simple translation into complex general motion of the upper platform.

5.2 First experimental scenario

The Stewart platform is tasked with obtaining a specific position measured in mm and orientation measured in degrees inside its workspace with its upper platform while the lower platform is kept stationary, as follows:

$$\begin{aligned} q_B &= \begin{bmatrix} 0 & 0 & 0 & 0 & 0 & 0 \end{bmatrix}^T \\ q_U &= \begin{bmatrix} 0 & 0 & 25+415.706 & 0° & 0° & 30° \end{bmatrix}^T \end{aligned} \tag{56}$$

For all six linear actuators, the steady-state error of displacements ess_i is a key performance parameter for evaluating the precision and stability of the positioning of the platform as used in many applications like radars. After the system reaches a stable state, it indicates the difference between desired and accomplished displacements. As shown in (Fig. 28), the linear actuators hold their target once they have settled.

The platform effectively tracks and maintains the intended position and orientation with a low steady-state error, assuring accuracy and dependability in its operation.

The steady state error values for the six linear actuators and its mean value in the first experimental scenario E1 as follows:

$$\begin{aligned} &ess_1 = 0.11cm \quad ess_2 = 0.07cm \\ &ess_3 = 0.10cm \quad ess_4 = 0.08cm \\ &ess_5 = 0.17cm \quad ess_6 = 0.09cm \\ &E_1 = 0.103cm \end{aligned} \tag{57}$$

The measured rotation angles of the upper platform provide information on how it has been rotated or oriented in relation to its reference position.

It is possible to monitor the ability of the upper platform to maintain precise orientations by recording its rotation angles.

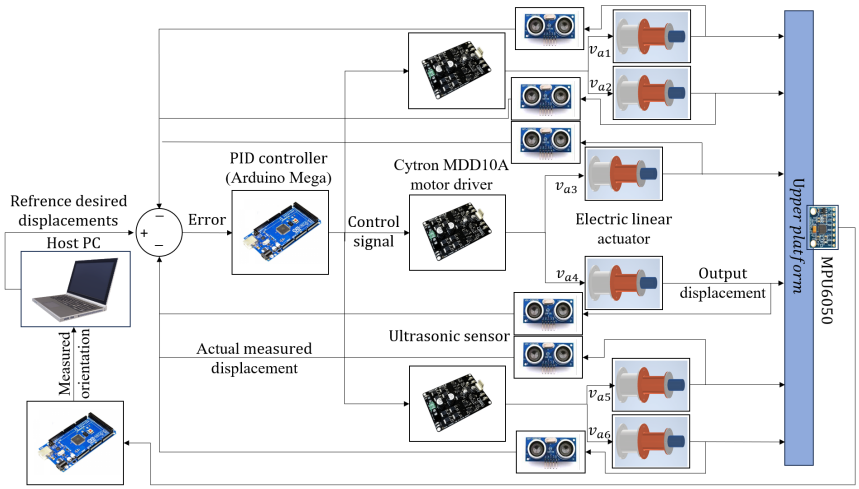

Figure 30. Wiring diagram of Stewart platform

As shown in (Fig. 31), rotation angles of the upper platform at the end of first scenario are −0.61°, 1.36° and 31.4° about x, y and z axis respectively with average error equal to 1.12° relative to the desired rotation angles.

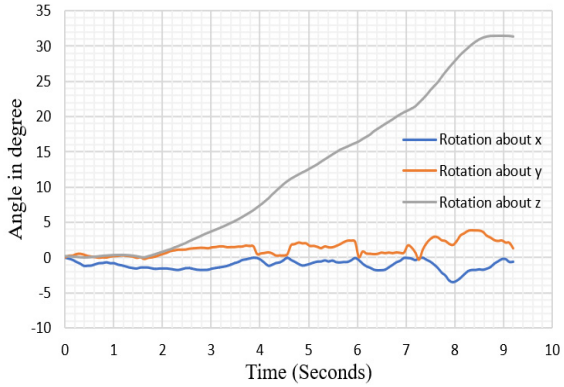

Figure 31. Rotation angles of first experimental scenario

As shown in (Fig. 32), the final position and orient–ation, as represented in both the SimMechanics simu–lation and the experimental model, exhibit a remarkable degree of similarity at the end of first experimental scenario.

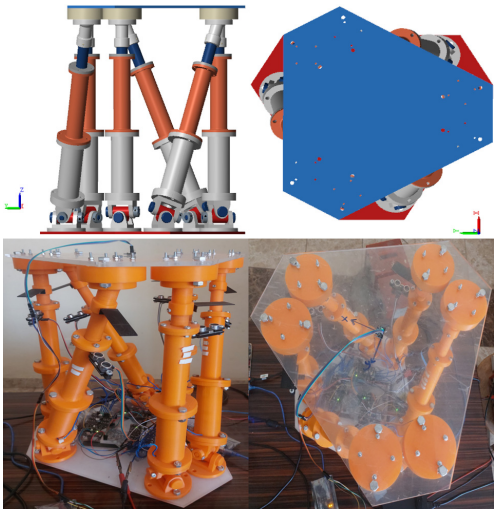

Figure 32. Simulated and experimental position and orientation of first experimental scenario

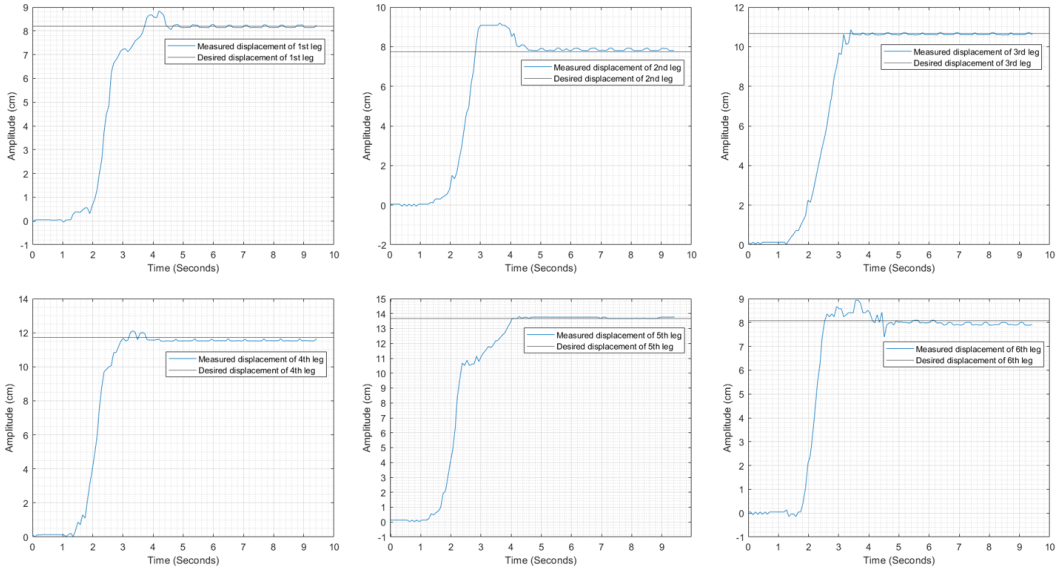

Figure 33. Electric linear actuators response to desired displacements in second experimental scenario

5.3 Second experimental scenario

The desired position measured in mm and rotation angles measured in degrees of the upper platform while keeping the lower platform still are illustrated as follows:

$$q_B = \begin{bmatrix} 0 & 0 & 0 & 0 & 0 & 0 \end{bmatrix}^T$$
$$q_U = \begin{bmatrix} -15 & 15 & 100+415.706 & -5° & 7° & -15° \end{bmatrix}^T \quad (58)$$

The linear actuators remain in their positions once they have settled, as seen in (Fig. 33).

The steady state error values for the six linear actuators and its mean value in the second scenario E2 are represented as follows:

$$ess_1 = 0.04cm \quad ess_2 = 0.06cm$$
$$ess_3 = 0.07cm \quad ess_4 = 0.09cm$$
$$ess_5 = 0.09cm \quad ess_6 = 0.16cm \quad (59)$$
$$E_1 = 0.085cm$$

As shown in (Fig. 34), the rotation angles of the upper platform at the conclusion of the fifth scenario are measured as −6.72°, 5.57°, and −14.65° about the x, y, and z axes, respectively, with an average error of 1.17° relative to the desired rotation angles. This data underscores the platform's precision in achieving the targeted orientations.

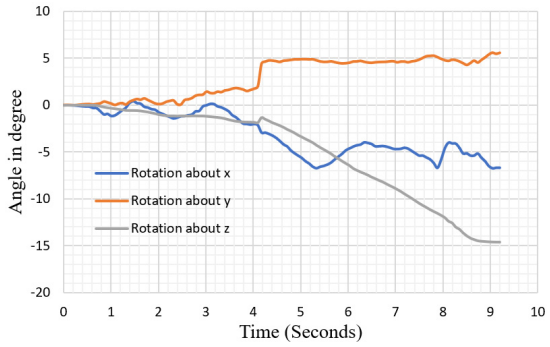

Figure 34. Rotation angles of second experimental scenario

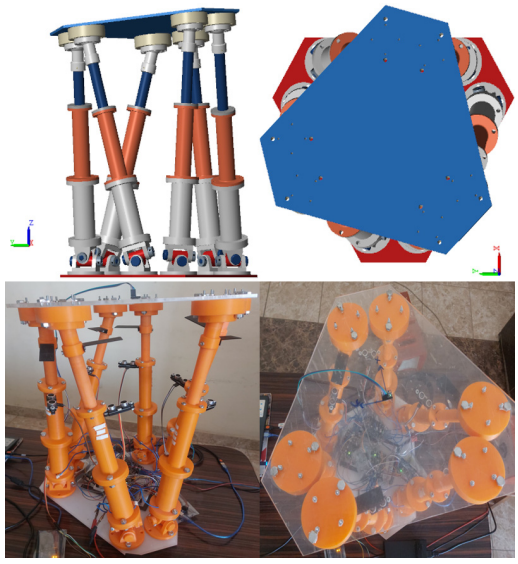

Figure 35. Simulated and experimental position and orientation of second experimental scenario

A comprehensive view of the final position and orientation of second scenario shown in (Fig. 35), aligning both the SimMechanics simulation and the experimental model, showcasing their remarkable similarity and validating the simulation's accuracy against real-world performance.

The total average error in displacement during the two experimental scenarios $E_{average}$, could be calculated as follows:

$$E_{average} = \frac{E_1 + E_2}{2} = 0.094cm$$

Similarly, the total average error in rotation angles during the two experimental scenarios is 1.145°.

The simulation model's utility within the setting of the experimental platform is expressed by the strong similarity between the simulation and experimental outcomes.

The analysis and validation of experimental models are significantly impacted by this harmonic convergence.

6. CONCLUSION

This paper presents an improved inverse kinematic model. It allows applying inverse kinematic analysis to any (UPS) Stewart model without the need for complex analytical methods. General motion of both upper and lower platforms has been considered in the generalized kinematic mathematical model.

Simulation analysis and numerical solutions are based on the use of SimMechanics with the aid of INVENTOR. Workspace analysis of the platform has shown the per–missible 3D range of each leg and its intersection consists the total range of the upper platform. Numerical and simulation analysis takes into account base motion during the first scenario. Analysis of path tracking in the second scenario has shown that position track error hadn't exceeded 10% along any axis while orientation error hadn't exceeded 2.32% about any axis. The analysis of errors in both position and orientation has assured model validation between both numerical and simulated results.

The total average error in displacement during the two experimental scenarios is $E_{average}$ = 0.094cm, while, the total average error in rotation angles during five scenarios is 1.145°. The simulation analysis and the experimental platform results are expressed by the strong similarity between the simulation and experimental outcomes.

REFERENCES

[1] P. Lingampally and A. Selvakumar, "A kinematic and workspace analysis of a parallel rehabilitation device for head-neck injured patients," FME Transactions, vol. 47, no. 3, pp. 405–411, 2019.

[2] E. Ibrahim, Tarek Elnady, M. Hassan, I. Saleh, "Modelling, transient response and hydraulic beha–viour of 2DOF stabilization platform," FME Tran–sactions, vol. 48, no. 4, pp. 833–840, Jan. 2020.

[3] Wikipedia, the free encyclopedia, "Amiba", 2006. [Online; accessed October 22, 2008].

[4] Wikipedia, the free encyclopedia, "Full flight simulator", 2013. [Online; accessed July 19, 2013].

[5] M. Wapler, V. Urban, T. Weisener, J. Stallkamp, M. Durr, and A. Hiller, “A stewart ¨ platform for precision surgery”, Transactions of the Institute of Measurement and Control, vol. 25, no. 4, p 329–334, 2003.

[6] V. R. Bolzon, T. L. Costa, E. H. Koroishi, and F. A. Lara-Molina, “Dynamic model and optimal control of a fully parallel manipulator”, International Journal of Engineering Research and Technology - IJERT, vol. 5, p 627–632, September 2016.

[7] K. Harib and K. Srinivasan, “Kinematic and dynamic analysis of stewart platform-based machine tool structures”, Robotica, vol. 21, p 541–554, 09 2003.

[8] Nikola Slavković, Saša Živanović, Nikola Vorkapić, and Zoran Dimić, “Development of the programming and simulation system of 4-axis robot with hybrid kinematic,” FME Transactions, vol. 50, no. 3, pp. 403–411, Jan. 2022.

[9] S. Pedrammehr, M. Mahboubkhah, and S. Pakzad, “An improved solution to the inverse dynamics of the general stewart platform”, in 2011 IEEE International Conference on Mechatronics, p 392–397, 2011.

[10] H. Guo and H. Li, “Dynamic analysis and simulation of a six degree of freedom stewart platform manipulator”, Proceedings of The Institution of Mechanical Engineers Part C-journal of Mechanical Engineering Science - Proc Inst Mech Eng C-J Mech E, vol. 220, p 61–72, 01 2006.

[11] H. Kalani and A. Akbarzadeh, “Improved general solution for the dynamic modeling of gough-stewart platform based on principle of virtual work”, Nonlinear Dynamics, vol. 83, p 2393–2418, 03 2016.

[12] B. Dasgupta and T. Mruthyunjaya, “The stewart platform manipulator: a review”, Mechanism and Machine Theory, vol. 35, no. 1, p 15–40, 2000.

[13] Z. Zheng, X. Zhang, J. Zhang, and Z. Chang, “A stable platform to compensate motion of ship based on stewart mechanism”, in Intelligent Robotics and Applications (H. Liu, N. Kubota, X. Zhu, R. Dillmann, and D. Zhou, eds.), (Cham), p 156–164, Springer International Publishing, 2015.

[14] D. Stewart, “A platform with six degrees of freedom”, Proceedings of the Institution of Mechanical Engineers, vol. 180, no. 1, p 371–386, 1965.

[15] D. Mendez, E. Lugo, M. Arias-Montiel, and R. Garcia Garcia, “Adams-matlab co-simulation for kinematics, dynamics, and control of the stewart–gough platform”, International Journal of Advanced Robotic Systems, vol. 14, p 172988141771982, 07 2017.

[16] J. Ding, C. Wang, and H. Wu, “Accuracy Analysis of Redundantly Actuated and Overconstrained Parallel Mechanisms With Actuation Errors”, Journal of Mechanisms and Robotics, vol. 10, 09 2018. 061010.

[17] J. He, H. Gu, and Z. Wang, “Solving the forward kinematics problem of six-dof stewart platform using multi-task gaussian process”, Proceedings of the Institution of Mechanical Engineers, Part C: Journal of Mechanical Engineering Science, vol. 227, p 161–169, 01 2013.

[18] M. Slavutin, A. Sheffer, O. Shai, and Y. Reich, “A Complete Geometric Singular Characterization of the 6/6 Stewart Platform”, Journal of Mechanisms and Robotics, vol. 10, 06 2018. 041011.

[19] Z. He, X. Feng, Y. Zhu, Z. Yu, Z. Li, Y. Zhang, Y. Wang, P. Wang, and L. Zhao, “Progress of Stewart vibration platform in aerospace micro–vibration control”, Aerospace, Volume 9, No. 6, p 324, pp. 1-20, 2022.

[20] T. R. Peterson, Design and Implementation of Stewart Platform Robot for Robotics Course Laboratory. Ph. D. dissertation, 2020. Copyright - Database copyright ProQuest LLC; ProQuest does not claim copyright in the individual underlying works; Last updated - 2023-08-15.

[21] C. Ophaswongse, R. C. Murray, and S. K. Agrawal, “Wrench Capability of a Stewart Platform With Series Elastic Actuators”, Journal of Mechanisms and Robotics, vol. 10, 01 2018. 021002.

[22] P. Donelan, Kinematic singularities of robot manipulators. INTECH Open Access Publisher, 2010.

[23] C. Ophaswongse, R. C. Murray, and S. K. Agrawal, “Wrench Capability of a Stewart Platform With Series Elastic Actuators”, Journal of Mechanisms and Robotics, vol. 10, 01 2018. 021002.

[24] J. McCarthy and G. Soh, Geometric Design of Linkages, vol. 11. 01 2011.

[25] A. Bahrami, M. Tafaoli-Masoule, and M. Bahrami, “Fuzzy control of piezoelectric stewart platform for active vibration control purpose”, TSEST, Transaction on Control and Mechanical Systems, p 356–361, 2012.

[26] Mohamed MR, Roshdy AA, Ali AA, Fayed MA. Position control of Stewart platform with electric linear actuator. In Journal of Physics: Conference Series 2023 Nov 1 (Vol. 2616, No. 1, p. 012027). IOP Publishing.

NOMENCLATURE

Roman Symbols

{abs}	The absolute fixed frame [x – y – z] attached to the platform center at O_{abs}
{B}	The lower platform frame [x_1 – y_1 – z_1] attached to the platform center at O_B
$\{f_i\}$	Local coordinate frame [x_{3i} – y_{3i} – z_{3i}] attached to the ith leg at O_i
$\{U\}$	The upper platform frame [x_2 – y_2 – z_2] attached to the platform center at O_U
a_i	The ith leg linear acceleration
$\vec{a}_{OB}^{abs}$	Acceleration vector of the lower platform center with respect to the absolute frame

$\vec{a}_{O_i}^{abs}$	Acceleration of leg connection point O_i with lower platform with respect to the absolute frame
$\vec{a}_{OU}^{abs}$	Acceleration vector of the upper platform center with respect to the absolute frame
$\vec{a}_{P_i}^{abs}$	Acceleration of leg connection point P_i with upper platform with respect to the absolute frame
$\vec{a}_{Ui}$	Acceleration of ith leg upper mass enter with respect to the absolute frame
D_i	Travel displacement of each linear actuator
ess_i	The steady-state error of displacements of linear actuators
$E_{average}$	The total average error in displacement during all scenarios
E_i	Mean error value in the ith scenario
$\hat{e}_i$	The ith leg unit vector with respect to the absolute frame
$\hat{e}_i^{fi}$	The ith leg unit vector with respect to the ith leg local frame
F_i^{dof}	Degrees of freedom of each joint
i	Leg order (i=1,2,3,4,5,6)
$I_{passive}$	Passive degrees of freedom of the mechanism
j	Total number of joints
J_1,J_2	Matrices associated with velocity mapping for the upper and lower platform respectively
J_B	Inverse Jacobian matrix of lower platform
J_{B1}, J_{B11}	Type one and type two of inverse Jacobian matrix associated with lower platform
J_U	Inverse Jacobian matrix of upper platform
J_{U1}, J_{U11}	Type one and type two of inverse Jacobian matrix associated with upper platform
l_i	The ith leg length (Euclidean distance)
n	Total number of links
N	Effective number of degrees of freedom of the mechanism
$\vec{O}_i^{abs}$	Position of the leg bottom with respect to the absolute frame
$\vec{O}_i^B$	Position vector of the ith leg bottom connection with the lower platform with respect to its local frame
$\vec{P}_i^{abs}$	Position of the leg tip with respect to the absolute frame
$\vec{P}_i^U$	Position vector of the ith leg tip connection with the upper platform with respect to its local frame
$\vec{P}_{OB}^{abs}$	Position vector of the lower platform center relative to the absolute frame
$\vec{P}_{OU}^{abs}$	Position vector of the upper platform center relative to the absolute frame
q_B	Total position and orientation vector of the lower platform
q_U	Total position and orientation vector of the upper platform
$\dot{q}_B$	Velocity mapping from the lower platform center to the ith leg connection with the lower platform relative to the absolute frame
$\dot{q}_U$	Velocity mapping from the upper platform center to the ith leg connection with the upper platform relative to the absolute frame
$\vec{q}_i^{abs}$	Position vector of ith leg tip with respect to upper platform center in the absolute frame
r	Circle radius
R_B	Matrix associated with lower platform angular velocity
R_B^{abs}	Rotation matrix of lower platform
R_{fi}^{abs}	Rotation matrix of ith leg frame
Ri	Matrix associated with ith leg angular velocity
R_U	Matrix associated with upper platform angular velocity
R_U^{abs}	Rotation matrix of upper platform
$\vec{r}_i$	Position vector of each leg
S_i^{abs}	Position vector of ith leg bottom with respect to lower platform center in the absolute frame
T_B^{abs}	Transformation matrix of the lower platform
T_U^{abs}	Transformation matrix of the upper platform
V_i	The ith leg linear speed
$\vec{V}_i^{abs}$	The ith leg linear velocity with respect to the absolute frame
$\vec{V}_{O_i/OB}$	Relative velocity of leg connection point O_i to lower platform center with respect to the absolute frame
$\vec{V}_{P_i}^{abs}$	Velocity of bottom connection O_i with respect to the absolute frame
$\vec{V}_{OB}^{abs}$	Velocity vector of the lower platform center with respect to the absolute frame
$\vec{V}_{OU}^{abs}$	Velocity of the upper platform center with respect to the absolute frame
$\vec{V}_{P_i/OU}^{abs}$	Velocity of P_i relative to upper platform center with respect to the absolute frame
$\vec{V}_{P_i}^{abs}$	Velocity of tip connection P_i relative to the absolute frame
$\vec{V}_{P_i/OU}^{abs}$	Relative velocity vector between leg upper point P_i and lower point O_i with respect to the absolute frame

Greek Symbols

α_{Bi}	Angle that $\vec{O}_i^B$ makes with x_1 axis in [x_1,y_1] plane
$\vec{\alpha}_i^{abs}$	Angular acceleration of ith leg with respect to the absolute frame
$\vec{\alpha}_{OB}^{abs}$	Lower platform angular acceleration with respect to the absolute frame
$\vec{\alpha}_{OU}^{abs}$	Upper platform angular acceleration with respect to the absolute frame
α_{Ui}	Angle that $\vec{P}_i^U$ makes with x_2 axis in [x_2,y_2] plane
γ_i	Rotation angle of ith passive universal joint about y_{3i}
θ_i	Rotation angles of ith leg frame
θ_{OB}	Local rotations of lower platform frame
θ_{OU}	Local rotations of upper platform frame
λ	Degrees of freedom of the space in which the mechanism operates
ψ_i	Rotation angle of ith passive U-joint about x_{3i}

$\vec{\omega}_i^{abs}$ Angular velocity of ith leg with respect to the absolute frame

$\vec{\omega}_{OB}^{abs}$ Lower platform angular velocity with respect to the absolute frame

$\vec{\omega}_{OU}^{abs}$ Upper platform angular velocity with respect to the absolute frame

УКЉУЧИВАЊЕ КРЕТАЊА ГОРЊЕ И ДОЊЕ ПЛАТФОРМЕ: ГЕНЕРАЛИЗОВАНИ ИНВЕРЗНИ КИНЕМАТИЧКИ МОДЕЛ ЗА СИМУЛАЦИЈУ И ЕКСПЕРИМЕНТАЛНО ТЕСТИРАЊЕ 6-УПС СТЈУАРТ ПЛАТФОРМЕ

М.Р. Мохамед, А.А. Али

Због тачности и прецизности паралелних мани–пулатора попут Стјуартове платформе, неколико технолошких апликација се ослања на њих. Мора се развити тачан кинематички модел како би се побољшала тачност манипулатора. У овом раду је извршено испитивање и верификација инверзног кинематичког модела. Спровођење и горње и доње платформе под различитим типовима кретања је одлика овог модела. 3D модел платформе је дирек–тно повезан са SimMechanics, отварајући пут за анализу симулације. За кодирање добијеног кинема–тичког модела коришћен је МАТЛАБ. Анализа радног простора платформе показала је дозвољени 3D домет сваке ноге, а њен пресек чини укупан домет горње платформе. Анализа симулације је показала да грешка позиционог трага није премашила 10% ни по једној оси, док грешка у оријентацији није премашила 2,32% ни по једној оси. У тесту експерименталног модела укупна просечна грешка у померању актуатора је 0,094 cm, док је укупна просечна грешка у угловима ротације 1,145°.